Title: Chromosomal rearrangements and segmental deletions contribute to gene loss in squamates

Buddhabhushan Girish Salve, Sonal H, Nagarjun Vijay

buddhabhushan21@iiserb.ac.in, sonal24@iiserb.ac.in, nagarjun@iiserb.ac.in

Computational Evolutionary Genomics Lab, Department of Biological Sciences, IISER Bhopal, Bhauri, Madhya Pradesh, India

Author for Correspondence: Nagarjun Vijay, nagarjun@iiserb.ac.in

Abstract

Background

Genomic rearrangements, including segmental deletions, duplications, translocations, and inversions of DNA segments, can contribute to gene losses, thereby reshaping genome architecture and potentially resulting in functional consequences. In squamates, karyotypic evolution mainly involves chromosome number reduction through fusions and microchromosome to macrochromosome translocations, although fissions have also contributed to diversification in several lineages. Despite these dynamics, the evolutionary processes and underlying genetic mechanisms driving chromosomal rearrangements and associated gene losses in squamates remain poorly understood.

Results

In this study, we analysed chromosome/scaffold-level assemblies of 261 squamates, corroborated by short-read, long-read, and transcriptomic data. We found multiple lines of evidence for the putative loss of 53 genes in the squamate lineage. Synteny and phylogenetic

analysis revealed that, among the 53 unretrieved orthologs, 14 are lost in squamates with no retained paralog, 15 show ortholog loss with retained paralogs, and 24 remain as unretrieved orthologs. Furthermore, we find that many of the genes lost from squamates are organised in syntenic clusters and are involved in essential immune functions—raising important questions about the role of paralogs in compensating for the function of lost genes, strengthening the "less is more" hypothesis in the squamate lineage.

Conclusions

Together, our comparative genomic analyses highlight that the loss of crucial genes in squamate lineages has occurred primarily through inter- and intrachromosomal rearrangements, including segmental deletions. These findings offer insights into the evolutionary loss of genes involved in macrophage differentiation and inform the development of novel pharmaceutical approaches for modulating immune responses.

Keywords

segmental deletions, macrophage polarisation, gene loss, karyotype evolution, squamates

Background

Genomic rearrangements, including deletions, inversions, translocations, and duplications, play a major role in shaping genome architecture and can potentially contribute to gene loss [1–3]. Such structural changes often disrupt gene integrity by breaking coding regions, altering regulatory landscapes, or relocating genes into heterochromatic or transcriptionally silent regions [4, 5]. For example, large-scale deletions can physically remove entire genes, whereas rearrangements such as translocations or inversions may separate essential gene components or place them under incompatible regulatory control, rendering them non-functional [3, 6, 7]. Moreover, rearrangements mediated by repetitive elements can create unstable genomic regions prone to further structural variation, thereby accelerating gene

erosion [8–12]. These processes are particularly evident in rapidly evolving lineages, such as birds and mammals, where gene loss contributes to lineage-specific adaptation and diversification [13–16].

The recent dramatic increase in the number of high-quality genome assemblies of diverse organisms has facilitated studies on lineage-specific gene losses [17–20]. The NCBI RefSeq annotation of orthologues for multiple vertebrate species and the availability of short- and long-read sequencing data allow the confirmation of gene losses [21, 22]. However, most studies linking gene loss and genomic rearrangements in vertebrate evolution have focused on birds [3, 23], mammals [11] and fishes [24], and the association of such chromosomal rearrangement and gene loss have not been systematically performed in squamates.

Squamate reptiles are a diverse monophyletic group of vertebrates classified into lizard and snake families, which diverged from tuatara approximately 250 million years ago (MYA) [25, 26]. With more than 11,000 described species, they are more species-rich than birds [27]. Squamates have emerged as excellent systems for studying genomic rearrangement [28], karyotype [29], genome size evolution [30], and unique biology such as tissue regeneration and limb degeneration [31, 32]. Yet, the dearth of genome assemblies has been a bottleneck for large-scale comparative genomic studies [33]. The recent availability of high-quality genomes across the squamate tree of life has opened new avenues to look at lineage-specific genome dynamics, such as sex chromosome evolution [34], changes in the repeat landscape [35], and GC content heterogeneity [36]. Notably, the genome size of squamates is heterogenous, with a trend toward genome size reduction [37]. Similar reductions in birds and bats have been associated with the loss of gene families and entire syntenic blocks, suggesting that the contraction of the gene repertoire may accompany genome size reduction [37, 38]. Although gene and whole-genome duplications drive evolutionary innovation, emerging evidence now reinforces the “less-is-more” hypothesis, highlighting gene loss as an

equally potent force in shaping genomic and phenotypic diversity [39–41]. The growing availability of chromosome-scale assemblies from initiatives such as the Vertebrate Genomes Project (VGP) is now enabling the systematic identification of such gene loss events, providing unprecedented opportunities to explore how gene reduction contributes to lineage-specific adaptation and evolutionary novelty [42–44]. In this context, investigating patterns of gene loss across the squamate radiation can therefore yield critical insights into how genomic reduction and restructuring contribute to phenotypic innovation, evolutionary diversification, and an alternative to phyletic gradualism [45].

To address this gap, we focused on gene loss in squamates and the role of genomic rearrangements. Our preliminary genome-wide screening of vertebrates revealed that 53 key genes with conserved functions are not annotated in NCBI RefSeq in squamates. Among these genes, previous studies have reported the loss of *PLAAT1*, *SLC24A1*, and *IL34* in squamates and associated them with adaptation to low-light environments [46], changes in the visual system [47], and myeloid cell-type evolution [48], respectively. These studies suggest the evolutionary loss of these genes based on a search of the genome assemblies and failure to recover any remnants. Here, we leverage high-quality genomes of squamates coupled with a comprehensive search of genomic short- and long-read and transcriptomic data, assembly validation, syntenic and phylogenetic analysis to rule out inadequacies in the genome assembly posing as gene loss [42, 49, 50]. We began our search by looking for genes annotated in the five outgroup species (i.e., Western clawed frog (*Xenopus tropicalis*), American alligator (*Alligator mississippiensis*), chicken (*Gallus gallus*), green sea turtle (*Chelonia mydas*), and human (*Homo sapiens*)) and not annotated in all annotated squamate genomes. Furthermore, we looked for direct (search of genomes, raw read datasets, statistical and phylogenetic signal of gene loss) and indirect evidence (co-evolution of the receptor) supporting the loss of these genes. We found that gene loss in squamates occurred in

conserved syntenic clusters, similar to the pattern observed in birds [38]. The putative gene loss we identified needs to be evaluated with better-quality genome assemblies, and its functional impact should be assessed through comparative functional assays.

Results

First, as a pilot analysis to identify unretrieved orthologs specific to the entire squamate lineage, we focused on genes consistently identified as not annotated in NCBI RefSeq across all 30 annotated squamate genomes, while being present in outgroup species (Additional file 1: Table S1-S2). To ensure robust inference, we used high-quality genome assemblies from multiple vertebrate species, including 261 squamates. Of these, 77 assemblies meet the quality standards recommended by global initiatives such as the Vertebrate Genome Project and the Earth BioGenome Project, with contig N50 values exceeding 1 Mb and scaffold N50 values exceeding 10 Mb (Additional file 1: Table S3). The 53 unretrieved orthologs were systematically classified into distinct categories based on multiple lines of genomic and syntenic evidence. These included: (i) assembly verification using long-read data through the Klumpy tool, (ii) local synteny assessment, (iii) evidence for segmental deletion or chromosomal rearrangement, (iv) ortholog sequence properties such as GC-content distribution and sequence identity with human orthologs, (v) local assembly using HybPiper followed by phylogenetic analysis, (vi) pairwise genome alignment, (vii) paralog annotation, (viii) transcriptional activity at the syntenic locus and cross-species expression mapping in central bearded dragon and chicken, (ix) BLASTn and tBLASTx searches in the near T2T phased genome assembly of central bearded dragon, and (x) BLASTn search against 261 squamate genomes. Based on the integration of syntenic and phylogenetic evidence, unretrieved orthologs were further subdivided into three categories: (i) ortholog loss with no retained paralog, supported by evidence for segmental deletion and/or syntenic and phylogenetic analysis and GC-content < 65% and sequence identity > 55% with no sequence

paralog found, (ii) putative ortholog loss with retained paralog, syntenic and phylogenetic analysis found paralog along with loss of orthologs, and (iii) unclear cases, where high sequence divergence for highly diverged ortholog or translocated ortholog with high sequence divergence or germline-restricted genes or hard to sequence genomic regions containing unretrieved orthologs present in dark matter or non-B-form DNA structures or proximity to telomeric and centromeric regions, prevented confident classification (Additional file 1: Table S1 and Additional file 2: Gene-wise evidences).

Unretrieved orthologs occur in conserved syntenic blocks and chromosomal rearrangements

We examined the genomic locations of the unretrieved orthologs in the chicken genome and found that they are distributed across both macro- and microchromosomes (**Fig. 1**). This contrasts with previous studies on gene loss in birds, where unretrieved orthologs were predominantly located on microchromosomes [38, 42]. We found clusters of unretrieved orthologs on chromosomes 1 (*LCP1*, *RUBCNL*, *SIAH3*, *LRCH1*, *ARL11*, *DLEU7*, *STOML3*, *INTS6* and *FREM2*) and 4 (*TBC1D14*, *MAN2B2*, *GPR78*, *GRK4*, *TNIP2*, *KDM3A*) of chicken. We also noted 7 clusters of two or more genes within ~ 2 Mb of each other in the chicken genome. The cross-species comparison of syntenic loci revealed that these regions are prone to both intra- and inter-chromosomal rearrangements in squamate species such as the central bearded dragon (*Pogona vitticeps*), brown anole (*Anolis sagrei*), and terrestrial garter snake (*Thamnophis elegans*) (**Fig. 1**; Additional file 1: Table S4). In several cases, these loci are also mapped to telomeric regions. In contrast, comparable rearrangements were not observed in other reptiles, including the American alligator (*Alligator mississippiensis*) and the green sea turtle (*Chelonia mydas*), suggesting squamate-specific genomic rearrangements.

Integrated multi-evidence stratified framework for putative gene loss validation

Based on the syntenic analysis along with local genome assembly validation, the 53 unretrieved orthologs could be classified as putatively lost due to segmental deletions (n=36) and intra/inter chromosomal rearrangements (n=17) (**Fig. 2A**). In the case of segmental deletions, the evidence for the loss of the gene consists of squamate-specific phylogenetic signal of reduction in intergenic distance, genome blast coverage, and phylogenetic assessment of sequences assembled by HybPiper or retrieved by blast search. While in the case of chromosomal rearrangements, the evidence relied largely on syntenic and phylogenetic analysis. An evidence score for the loss of each gene based on these integrated multiple layers of evidence was used to rank the unretrieved orthologs.

The BLASTn search of 261 squamate genomes revealed that most unretrieved orthologs are absent from squamates. Of the 53 genes, 21 have query coverage (search on squamate genomes using human orthologues as a query) of ≤ 25%, 23 genes between 25 - 74%, and 9 genes have coverage of ≥ 75% (*SUV39H2*, *FREM2*, *DNM3*, *RBBP7*, *MOB1A*, *SSTR4*, *WNT2*, *LCP1* and *CAV3*; **Fig. 2B**; Additional file 1: Table S5). Our bioinformatic analysis (using BioMart human paralog annotation) revealed two or more paralogs for each gene having query coverage >75% (**Fig. 3**; Additional file 1: Table S6). Furthermore, we assembled gene sequences using raw whole-genome sequencing datasets. The phylogenetic analysis of the retrieved sequences revealed that they cluster with closely related paralogues rather than the expected orthologues (Additional file 1: Table S7 and Additional file 2: Gene-wise evidences).

It has been previously reported that unretrieved orthologs or ”missing” or ”hidden” genes in genome assemblies are often associated with high GC content and high sequence divergence [42, 49, 51, 52]. However, in our analysis, the mean GC content of the unretrieved ortholog

(calculated across vertebrate orthologues) ranged from 39.56% to 64.72% (**Fig. 2B**). Notably, nineteen genes—*CAV3* (55.21%), *NOTCH2* (55.30%), *CYYR1* (55.43%), *DIP2A* (55.47%), *UNKL* (55.80%), *RIPPLY3* (56.06%), *ADRA1B* (56.48%), *IL34* (56.76%), *WNT2* (56.90%), *TNIP2* (57.83%), *SLC9A5* (58.12%), *MATK* (58.23%), *SIAH3* (58.52%), *DLEU7* (58.67%), *ARL11* (58.92%), *HSD17B1* (61.35%), *YBX3* (61.65%), *SH2D2A* (64.47%), and *SSTR4* (64.72%)—had GC content exceeding 55% (Additional file 1: Table S1).

Immune genes often evolve under strong selective pressure due to the ongoing evolutionary arms race between the host immune system and invading pathogens. This rapid evolution results in low amino acid conservation among orthologous proteins across species, limiting the effectiveness of sequence similarity-based tools such as BLASTn for detecting these genes [52–55]. Therefore, some of these genes may not be truly lost but may be present as highly diverged orthologs. We observed that 24 genes including *ARL11, GPR78, HHLA2, HPGDS, HSD17B1, IFTAP, IL13RA2, IL26, MATK, MOB1A, OLAH, PLAAT1, RBBP7, SH2D2A, SLC24A1, TMEM273, UTS2B, ZNF438, DLEU7, DNM3, UNKL, MAN2B2, RUBCNL, and TNIP2* share less than 65% sequence identity with their human orthologs (**Fig. 2B**; Additional file 1: Table S1), suggesting that moderate to high sequence divergence may contribute to their loss or lack of annotation in squamate genomes, therefore remained classified as unretrieved orthologs. Comparative genome alignment between human and tuatara reveals that several genes were intact in the ancestral lineage with conserved gene synteny, highlighting their loss as specific to squamates (Additional File 1: Table S8).

Based on syntenic analysis, 36 genes were found to have a conserved gene order similar to that of the outgroup species, while eight genes showed evidence of intrachromosomal rearrangements and nine genes indicated interchromosomal rearrangements (**Fig. 2A**; Additional file 1: Table S1). Most of the 53 unretrieved orthologs lacked evidence of transcription, with some genes having spurious mapping (Additional File 3: Cross species

RNA-seq mapping). We found evidence for segmental deletion in the case of 19 out of 36 genes, namely, *ADAP2*, *ELOVL3*, *GRK4*, *HHLA2*, *HSD17B1*, *IL34*, *IL5RA*, *KDM3A*, *LAPTM5*, *MOB1A*, *RBBP7*, *RIPPLY3*, *SLC24A1*, *SLC9A5*, *SSTR4*, *STAP1*, *SUV39H2*, *TBC1D14*, *TMEM273* and *WNT2* (Additional file 1: Table S1).

Paralogs were not found for 14 of the 53 unretrieved orthologs. Among these 14 genes, (i) *IL34*, *IL5RA*, and *RIPPLY3* exhibit high sequence divergence while retaining conserved synteny, with additional evidence of segmental deletion, (ii) A similar pattern (except for high sequence divergence) was observed for *GRK4*, *LAPTM5*, *SLC9A5*, *SSTR4*, *STAP1*, and *WNT2*, (iii) Despite weak evidence of segmental deletion, *CYYR1* (with frame-disrupting changes in *Anolis sagrei*, partial exon remnants in a genome assembly validated syntenic locus in *Pogona vitticeps* and lack of transcription in *Pogona vitticeps* and *Rhineura floridana*) and *GPR82* (with no blast hits even to paralogs despite low sequence divergence among orthologs) have conserved synteny (Additional file 4: Figure S1), (iv) The phylogenetic analysis suggests the lack of paralogs among the chromosomal rearrangement genes, *DIP2A*, *NOTCH2*, and *SH2D1A*. Collectively, these 14 genes were classified as cases of ortholog loss with no retained paralog (Additional file 1: Table S1, and Additional file 2: Gene-wise evidences).

Multi-gene families are often prone to inactivation or deletion, consistent with the birth-and-death model of gene family evolution [13, 24, 56, 57]. We found that 39 of the 53 unretrieved orthologs belong to multi-gene families and have at least one paralogue (**Fig. 2** and **Fig. 3**; Additional file 1: Table S1, S6 and S7). Among these 39 genes, (i) the evidence for conserved synteny and segmental deletion with limited sequence divergence was found for *ADAP2*, *CAV3*, *EVOVL3*, *INTS6*, *KDM3A*, *SUV39H2*, and *TBC1D14*, (ii) chromosomal rearrangement was identified in the case of *ADRA1B*, *KREMEN1*, *FREM2*, *LCP1*, *LRCH1*, *SIAH3*, *STOML3*, and *YBX3* with limited sequence divergence. Collectively, these 15 genes were

classified as cases of ortholog loss with retained paralog (Additional file 1: Table S1, and Additional file 2: Gene-wise evidences).

Of the remaining 24 of the 39 genes with paralogs, *ARL11*, *GPR78*, *HHLA2*, *HSD17B1*, *IFTAP*, *IL13RA2*, *IL26*, *OLAH*, *PLAAT1*, *SH2D2A*, *SLC24A1*, *TMEM273*, *UTS2B*, *DLEU7*, *UNKL*, *FREM2*, *LCP1*, *LRCH1*, *MAN2B2*, *RUBCNL*, *SIAH3*, *STOML3*, and *TNIP2* had high sequence divergence and remain as unretrieved orthologs. In summary, synteny and phylogenetic analyses suggest that, among the 53 unretrieved orthologs, 14 genes are lost in squamates with no retained paralog, 15 show ortholog loss with retained paralogs, and 24 remain as unretrieved orthologs (Additional file 1: Table S1, and Additional file 2: Gene-wise evidences).

Furthermore, pair-wise genome alignments (at these 53 unretrieved orthologs loci) between chicken (*Gallus gallus*) and 34 other vertebrate species revealed that the squamate (~280 MYA) genomes consistently having lower aligned exonic regions compared to tuatara (*Sphenodon punctatus*; ~280 MYA), Testudines (~261 MYA), and Crocodilians (~245 MYA), despite these groups having comparable evolutionary divergence from chicken (**Fig. 4A**; Additional file 1: Table S9 and Additional file 4: Figure S2; pair-wise divergence time obtained from Timetree website [58]). The flanking genes to focal genes show significantly higher levels of alignments at exonic regions (**Fig. 4B;** Additional file 1: Table S9, and Additional file 2: Gene-wise evidences). The ENSEMBL available and chains files (pair-wise genome-wide LASTZ alignment) created by this study do not show any marked difference (Wilcoxon, p-value = 0.16, **Fig. 4C**). We also found that the aligned regions at exonic positions of focal genes are significantly lower in squamates compared to Birds, Coelacanthiformes, Testudines, Crocodylia, and Sphenodontia **(Fig. 4D**, Additional file 1: Table S9). The occurrence of unaligned regions in non-squamate species for some genes

could be due to assembly gaps and/or high sequence divergence. The aligned region could also be from the paralogous regions.

Comparative genomic evidence for *IL34* loss via segmental deletion in squamates

As reported previously [48], our comparative genomic analysis confirmed the absence of the *IL34* gene in squamates despite its widespread conservation across other vertebrates. Synteny analysis revealed that *COG4* and *SF3B3* typically flank *IL34* on the left and *MTSS2* and *VAC14* on the right (**Fig. 5A**; Additional file 1: Table S4). Notable exceptions are observed in species such as the zebrafish (*Danio rerio*), green sea turtle (*Chelonia mydas*), American alligator (*Alligator mississippiensis*), and tiger rattlesnake (*Crotalus tigris*), which have *IONP2*, *PARD6A*, *BBS2*, and *CNOT1*, respectively, on the right flank of the *IL34* locus. The lack of annotation for the *IL34* gene in squamates could potentially result from assembly artefacts. To rule out this possibility, we examined the syntenic locus of *IL34* in squamate species such as the common wall lizard (*Podarcis muralis*) and the Indian cobra (*Naja naja*) using PacBio and Oxford Nanopore long-read data. In both cases, overlapping reads span the *IL34* gene locus, indicating that the assemblies are correct at this locus (**Fig. 6**). BLASTn analysis of squamate genome assemblies and raw read datasets failed to recover any sequence corresponding to the *IL34* gene, further supporting its absence in this lineage and ruling out the possibility of its translocation to another genomic region (Additional file 1: Table S5 and S7). Next, we compared intergenic distances by examining squamate species for evidence of segmental deletions compared to non-squamate species (see Methods). Wilcoxon rank-sum tests (alternative = "less") consistently yielded adjusted p-values < 0.001 for all combinations of gene distance ratios involving *SF3B3–MTSS2*, indicating significant contraction in this region in squamates (**Fig. 5B**; Additional file 1: Table S1; Additional file 4: Fig. S3). In contrast, other gene combinations did not significantly differ across all comparisons. Additionally, evidence for segmental deletion was supported by phylogenetic logistic

regression analyses, with significant results from both logistic_MPLE (slope = 0.2; *p*-value = 0.0022) and logistic_IG10 (slope = 0.2; *p*-value = 0.0018) (**Fig. 5C**; Additional file 1: Table S1). Additionally, we found intrachromosomal rearrangement of the *IL34* locus in some of the Viperidae snake species (Additional file 4: Fig. S4).

Our bioinformatic analysis, integrating synteny, long-read mapping-based genome assembly verification, BLASTn searches, transcriptome searches, intergenic distance comparisons, and phylogenetic regression, robustly confirms the loss of the *IL34* gene in squamates.

Co-evolution of *CSF1R* with *IL34* gene loss in the squamate lineage

Our previous results from multifaceted approaches concurrently infer loss of the *IL34* gene from squamates. Next, we investigated the evolutionary consequences of *IL34* gene loss on its receptor —*CSF1R*, in squamates. Previous studies have suggested that *IL34* remains relatively unchanged, with detectable co-variation with *CSF1R*, whereas no such correlation is observed for *CSF1* [Garceau et al. [59], reviewed in [60]]. However, this hypothesis remains untested in lineages where *IL34* is lost. The availability of high-quality genome assemblies of squamates and *IL34* gene loss opens the opportunity to address this interesting evolutionary question─how two ligands evolve with a single receptor? Using selection analysis tools, we detected signatures of relaxed selection acting on *CSF1R* in several squamate species. We found squamate species such as Western terrestrial garter snake (*Thamnophis elegans*; *p*-values = 0.0003, k-value = 0.63), komodo dragon (*Varanus komodoensis*; *p*-value = 0.0053, k-value = 0.62), and central bearded dragon (*Pogona vitticeps*; *p*-value = 0.0047, k-value = 0.59) show signatures of relaxed selection by RELAX (with *p*-values <0.05 and k-value <0) and/or codeml (**Fig. 7**; Additional file 1: Table S10). Notably, signatures of relaxed selection were not pervasive across the screened vertebrate lineages, suggesting lineage-specific evolutionary changes. Several sites within the

extracellular domain of *CSF1R* were identified as positively selected by both MEME and FEL analyses, with squamate species exhibiting a relatively higher number of positively selected sites (Additional file 1: Table S10). Together, the results of comparative sequence analyses revealed lineage-specific modifications in *CSF1R* in squamates, potentially reflecting compensatory evolution following *IL34* gene loss. These findings provide indirect but compelling evidence for *IL34* gene loss in squamates and support the hypothesis of receptor adaptation following the loss of one of its ligands.

Discussion

Our study identifies large-scale gene losses across squamates, with 53 genes consistently unretrievable in all 261 squamate genomes screened. These genes are dispersed across macro- and microchromosomes in the chicken genome and are typically lost individually, while some are unretrievable in clusters. Based on synteny conservation, the unretrieved orthologs are classified as putatively lost due to segmental deletions (n=36) and intra/inter chromosomal rearrangements (n=17). Among the 53 unretrieved orthologs, 21 had < 25% blastn query coverage, 23 had intermediate coverage of 25–74%, and 9 had ≥75% coverage in the genomes of squamates. The mean GC content of the unretrieved orthologs ranges from 39.56 % to 64.72 %, is within a GC-neutral range and suggests that GC bias is unlikely to cause them to be unretrievable. Additionally, many of these genes exhibit less than 70% sequence identity to their human orthologues, indicating substantial evolutionary sequence divergence. Despite extensive efforts, we could not recover these genes from available genomic or transcriptomic resources, including searches in high-quality genome assemblies, analyses of raw genomic sequencing reads, and examination of RNA-seq data across diverse tissues in the central bearded dragon (*Pogona vitticeps*). The synteny and phylogenetic analyses of the 53 unretrieved orthologs revealed that 14 genes are lost in squamates with no retained paralog, 15 show ortholog loss with retained paralogs, and 24 remain unretrieved orthologs.

Based on the evidence score, *IL34* is the strongest empirical case of evolutionary gene loss. Our comparative genomic analyses confirmed the complete loss of *IL34* in squamates via segmental deletion and intrachromosomal rearrangements at the *IL34* locus in some *Viperidae* snakes. We also identified squamate-specific modifications in *CSF1R*, suggesting possible compensatory changes following *IL34* loss. Similarly, *CAV3* and *KDM3A* have the highest evidence score among the 14 orthologs lost with retained paralogs. While the cross-species mapping found noisy RNA-seq support for both these genes, the phylogenetic analysis and synteny confirm the loss of the ortholog with the paralogs retained in line with the "less is more" hypothesis.

Evolutionary loss of conserved genes in squamates: patterns and limitations

In squamates, we discovered that segmental deletions and intra- and inter-chromosomal genomic rearrangements cause the putative loss of these 53 unretrieved orthologs. In contrast with previously documented gene losses in birds, which are primarily found on microchromosomes and are found to be due to assembly errors [42], these genes are dispersed throughout different macro- and microchromosomes rather than clustered on microchromosomes in the chicken genome [38, 61]. We observed that some gene losses occurred in clusters, with two or more adjacent genes unretrievable from the same genomic region. For *IL34*, both segmental deletions and intra-chromosomal rearrangements were observed, suggesting that these loci lie in structurally unstable regions. The loss of *IL34* in squamates, along with the signatures of loss on the receptor and presence of a structural paralog [48, 59, 62], makes the case for functional compensation by distant structural homologs [63, 64]. Sequence paralogs from ancient whole-genome or segmental duplications are more widely studied than structural homologs. The example of ortholog loss with retained paralog, such as *CAV3*, *KDM3A*, *ADAP2*, *SUV39H2*, and *TBC1D14*, could be compensated for by their paralogs, such as *CAV3*-like, *KDM3B*, *ADAP1L*, *SUV39H1* and *TBC1D12*.

Furthermore, the pattern of *TNIP2* presence in the vicinity of the telomeric region of chicken chromosome 4, compared to interchromosomal rearrangement in squamates (Additional file 4: Fig. S5), suggests that gene loss may be facilitated by the prevalence of the gene in highly variable and rapidly evolving regions such as telomeric and sub-telomeric regions [65, 66]. Genes such as *TNIP2* are retained as unretrieved orthologs due to the challenges of distinguishing evolutionary loss of genes from methodological limitations.

Previous studies [38, 52, 53, 61] have shown that some genes initially reported as “missing” in birds were later recovered using transcriptomic data [50], with their absence attributed to high GC content and limitations in earlier genome assemblies [49]. We incorporated GC content analysis to avoid similar errors, searched short- and long-read datasets, and examined RNA-seq data to minimise the risk of false gene loss inference in squamates. The GC content of unretrieved orthologs in squamates is less than that reported for the “missing” GC-rich genes in birds, which were later found to be “dark matter” missing in prior genome assemblies [42, 49, 67–69]. While lineage-specific GC content shifts in squamates cannot be ruled out, the presence of most unretrieved orthologs in tuatara weakens the likelihood of a widespread increase in GC content in squamates. Furthermore, we assembled gene sequences by performing BLASTn searches using raw whole-genome sequencing datasets. Phylogenetic analysis of the retrieved sequences revealed that they clustered with closely related paralogues rather than the expected orthologues. We verified genome assemblies for conserved synteny and ruled out assembly artefacts as the cause of unretrieved orthologs, suggesting that structural rearrangements, rather than assembly artefacts, may play a role in gene loss. Many of the unretrieved orthologs, including several interleukins, show less than 70% identity to their human orthologues and are primarily linked to immune functions (for gene-specific detailed references, see Additional file 1: Table S11). A plausible explanation is the involvement of these genes in host-pathogen arms races, where rapid evolution driven by

changing selective pressures can lead to high sequence divergence and positive selection [70–73]. Consequently, these genes may still exist in squamates but in highly diverged forms, making them difficult to detect using standard sequence homology-based approaches. Furthermore, we could not accurately estimate deletion sizes, as the genes are absent in all the examined squamates, and the nearest outgroup with intact genes, tuatara, diverged ~250 MYA [26]. This deep divergence limits the precise delineation of deletion boundaries, unlike in previous studies, where segmental deletions could be more clearly defined [6, 54].

The discovery of squamate-specific gene losses offers insights into their evolutionary importance, supporting the idea that gene loss can be adaptive and extending the "less-is-more" hypothesis to squamates vis-à-vis providing an alternative to phyletic gradualism [39, 65, 74–77]. Many unretrieved orthologs have multiple paralogs; in some cases, their apparent absence may result from assembly limitations. However, if the gene loss is true, its function is likely compensated by paralogous genes. Additionally, most unretrieved orthologs form conserved syntenic clusters in non-squamate vertebrates, suggesting their loss in squamates likely involved block deletions, potentially contributing to genome size reduction [37]. Future genome assemblies should aim to assess the presence or absence of these genes to understand the mechanisms and evolutionary consequences of their loss.

Functional implications of unretrieved orthologs

Earlier studies reported the absence of *PLAAT1*, *SLC24A1*, and *IL34* in squamates and associated their loss with adaptations to low-light environments, modifications in the visual system, and the evolution of myeloid cell types, respectively [46–48]. Our methodology has extended the search genome-wide and identified these genes as unretrieved orthologs, reinforcing the reliability of our gene loss detection approach and highlighting the need for detailed functional investigations of unretrieved orthologs. A literature survey revealed that

the 53 unretrieved orthologs from squamates are linked to diverse biological functions, including immunity and inflammation, cell growth, apoptosis, cancer, development, cardiovascular and metabolic processes, musculoskeletal formation, sensory function, and core cellular mechanisms like autophagy, protein degradation, and transcriptional regulation (for gene-specific detailed references, see Additional file 1: Table S11). The involvement of these genes in fundamental physiological and immune functions raises critical questions about how these pathways operate in their absence, offering a valuable opportunity to explore compensatory mechanisms and lineage-specific adaptations. The loss of these genes may play a pivotal role in evolutionary genetics by influencing genome size and complexity, affecting the rate of evolution and adaptation, offering insights into gene and pathway essentiality, and contributing to phenotypic diversity in squamates [13]. Furthermore, we found that the genes *KDM3A*, *SUV39H2*, and *RBBP7*, which are unretrieved in squamates, are associated with the Gene Ontology (GO) term "chromatin remodeling", and are involved in DNA replication, recombination, and repair. The absence of these genes suggests a potential impact on chromatin architecture, with possible consequences for genome accessibility and stability in squamates [3]. The genes *FREM2*, *WNT2* and *NOTCH2* involved in eye development are unretrieved and may be associated with changes in the visual system in squamates [31, 46, 47].

The present study reports the loss of four genes─ *IL34*, *STAP1*, *LAPTM5* and *TNIP2*- involved in macrophage activation and polarisation. *IL34* expression is observed in tissues such as the skin, brain, kidneys, and testes and is modulated in diseases like Alzheimer's, cancer and HBV viral infection [78–80]. The macrophages derived from *IL34* exhibit more anti-viral activity than those from *CSF1* [81–83]. Despite having a normal phenotype, *IL34*$^{-/-}$ mice exhibit impaired responses to skin antigens and viral infections, highlighting its physiological importance [84, 85]. These findings suggest that squamates may be

functionally compromised owing to the loss of *IL34*, potentially rendering them more susceptible to pathogenic infections. In mice, *STAP1* deficiency impairs TCR-mediated T cell activation [86], *TNIP2* acts as a regulator of NF-κB signalling [87, 88], and *LAPTM5* inhibits HIV-1 progeny infectivity by transporting viral Env to the lysosome for degradation in macrophages [89]. However, the role of these genes in reptiles remains largely unexplored and needs functional validation. The limited availability of tools for assessing immune function in free-living reptiles presents a challenge in functionally testing this scenario. These findings offer new insights into the evolutionary reduction in the gene repertoire regulating macrophage differentiation, which may help develop novel pharmaceutical strategies for the immune modulation of monocytes and macrophages.

Conclusions

This study systematically identified and confirmed that 53 genes are putatively lost in the squamate lineage but retained in outgroup species, suggesting lineage-specific gene loss events primarily associated with large-scale segmental deletions and chromosomal rearrangements. Among the 53 unretrieved orthologs, 14 genes are lost in squamates with no retained paralog, 15 show ortholog loss with retained paralogs, and 24 remain unretrieved orthologs. Notably, four unretrieved orthologs are involved in macrophage activation and polarisation—*IL34*, *STAP1*, *LAPTM5* and *TNIP2*, while others play key roles in immunity, development, metabolism, cellular processes, and neuronal and musculoskeletal functions. The unretrieved orthologs are GC-neutral and are members of multi-gene families with several paralogues. Our study provides direct and indirect evidence of potential gene losses in the squamate lineage. Despite comprehensive searches across genome assemblies, raw reads, and transcriptomes, none could be recovered, supporting their possible loss in squamates. Further studies are needed to generate high-quality squamate genomes to identify the causative forces behind these gene losses and their final confirmation.

Methods

Identification of unretrieved orthologs from squamates

We retrieved the list of all 20,595 protein-coding genes annotated in the human genome from NCBI (Additional file 1: Table S1-S2). The orthologues for each human gene across 679 annotated vertebrate genomes were obtained using the datasets command-line utility of NCBI (parameters: --ortholog all) [90]. First, as a pilot analysis to identify unretrieved orthologs specific to squamates, we focused on genes consistently identified as not annotated in NCBI RefSeq across all 30 annotated squamate genomes. As a filtering criterion to ensure that these genes were not universally absent or pseudogenised or annotation artefact, we retained only those genes that were classified as intact (annotated without the "Low quality protein" tag of NCBI) in multiple distantly related species, namely Western clawed frog (*Xenopus tropicalis*), American alligator (*Alligator mississippiensis*), chicken (*Gallus gallus*), green sea turtle (*Chelonia mydas*), and human (*Homo sapiens*) allowing to confidently infer squamate-specific unretrieved orthologs by comparing across a broad phylogenetic tree of vertebrates (Additional file 1: Table S1-S2).

Analysis of evolutionary rearrangement and chromosomal mapping of unretrieved orthologs

To investigate the chromosomal distribution and rearranged genomic regions of unretrieved orthologs across squamates, we mapped them to chicken karyotypes. We used GENESPACE v1.3.1 [91] to understand patterns of synteny and orthology across chicken (*Gallus gallus*), American alligator (*Alligator mississippiensis*), green sea turtle (*Chelonia mydas*), central bearded dragon *(Pogona vitticeps*), brown anole (*Anolis sagrei*), and terrestrial garter snake (*Thamnophis elegans*) genomes. A comparative framework enabled the visualisation of conserved syntenic blocks and rearranged genomic regions linked to these 53 unretrieved

orthologs in squamates. We used BEDTools nuc to calculate GC content across 100 bp sliding windows along the length of the chromosome. To identify sequences associated with non-B DNA-forming motifs, we used the GFA v2 program [92]. The resulting outputs were used to plot the GC content and the presence of non-B DNA motifs across chicken chromosomes. Additionally, the unretrieved orthologs loci were compared between the genome assemblies of chicken (*Gallus gallus*) and green anole (*Anolis carolinensis*) using the NCBI Comparative Genome Viewer [93].

BLASTn search of 53 unretrieved orthologs in squamate genomes and raw read datasets

To increase the power of screening for unretrieved orthologs in squamate genomes, we performed BLASTn [94] searches (parameters: -evalue 0.05 -outfmt '17 SQ', 1, 6, and 7) across 261 squamate genome assemblies, including both chromosome-level and scaffold-level assemblies, using human (*Homo sapiens*) and chicken (*Gallus gallus*) gene sequences as queries (Additional file 1: Table S5). The BLASTn output in format '17 SQ' was used to generate IGV reports [95], which were then screened to assess the presence of gene sequences in the squamate assemblies. Furthermore, we screened publicly available short- and long-read DNA and RNA sequencing data from PacBio (HiFi and Revio), Oxford Nanopore, and Illumina sequencing technologies—from squamate species (Additional file 1: Table S12). We employed BLASTn (parameters: -evalue 0.05 -max_target_seqs 10000) with query sequences of unretrieved orthologs of the five outgroup species. To distinguish between orthologs and paralogs, the sequence obtained from HybPiper [96] was analysed using IQ-TREE v2.3.6 [97], along with coding DNA sequences from 39 species that produced BLASTn hits to the extracted sequence (parameters: -evalue 0.001)(Additional file: Table S12). We used the 'ape' package to identify the closest phylogenetic branches to the HybPiper recovered gene sequence [98]. Similar phylogenetic analysis was performed using

newly available near-complete T2T genomes of the Australian central bearded dragon (*Pogona vitticeps*) [99, 100]. To identify orthologous genes across 28 species (19 squamates and 9 outgroups), protein sequences of all annotated genes in FASTA format were used as input to OrthoFinder 2 [101]. The analysis involved an all-vs-all sequence similarity search using DIAMOND, followed by clustering of genes into orthogroups, each representing a set of genes derived from a single ancestral gene in the last common ancestor. From this dataset, we focused on 53 genes of particular interest and retrieved their corresponding orthogroup IDs. The gene IDs within these orthogroups were then extracted. To confirm whether these sequences represented true orthologs, or paralogs, or gene duplicates, we conducted synteny analyses and phylogenetic inference using IQ-TREE 2 (Additional file 1: Table S13) [97].

Furthermore, to assess the paralog prevalence, we used Ensembl BioMart to obtain annotated paralogs, GC content, sequence identity, and transcript count data for human and chicken orthologs of squamate-specific unretrieved orthologs.

To explore potential transcriptional evidence for unretrieved orthologs, we mapped RNA-seq data from the central bearded dragon (*Pogona vitticeps*) of the testis, muscle, lung, liver, kidney, eye, heart, and brain tissues to the chicken genome using minimap2 v2.29-r1283 [102] (parameters: -ax splice -uf -k14) and FLAIR v2.2.0 [103] (Additional file 1: Table S12). We then screened for the presence of transcripts corresponding to unretrieved orthologs and visualised the read coverage and splice junctions using IGV-report, allowing us to assess transcriptional signals for these genes in the central bearded dragon (*Pogona vitticeps*) despite their apparent genomic absence (i.e., lack of annotation and failure to be picked up by blastn search).

Identification of 1-to-1 orthologs, assembly verification, GC content, paralog annotation of unretrieved orthologs

We confirmed gene synteny of unretrieved orthologs and identified 1-to-1 orthologs across eight vertebrate species, namely Western clawed frog (*Xenopus tropicalis*), American alligator (*Alligator mississippiensis*), chicken (*Gallus gallus*), green sea turtle (*Chelonia mydas*), green anole (*Anolis carolinensis*), Common wall lizard (*Podarcis muralis*), Central bearded dragon (*Pogona vitticeps*), Eastern brown snake (*Pseudonaja textilis*), tiger rattlesnake (*Crotalus tigris*), tuatara (*Sphenodon punctatus*), platypus (*Ornithorhynchus anatinus*), house mouse (*Mus musculus*) and human (*Homo sapiens*) using NCBI genome viewer [22] and ENSEMBL [104]. To assess the integrity of the unretrieved orthologs loci in the chromosome/scaffold-level assembly of Indian cobra (*Naja naja*), tiger rattlesnake (*Crotalus tigris*), Central bearded dragon (*Pogona vitticeps*) and common wall lizard (*Podarcis muralis*). We used the *scan_alignment* and *alignment_plot* options in the Klumpy v1.0.10 tool [105], the required BAM file was generated by mapping long-read sequencing data from squamates species (Additional file 1: Table S12) with Minimap2 v2.17-r941 [102] (parameters: -ax map-pb or -ax map-hifi or -ax map-ont). The resulting alignment plots were examined for the presence of continuous and overlapping reads spanning the unretrieved orthologs loci.

The lack of annotations and/or sequence for the unretrieved ortholog from the genome assembly of a species could be due to its high GC content and/or high sequence divergence [42, 49, 106]. Therefore, we calculated GC content across the coding sequence of vertebrate orthologs using seqkit (parameters: fx2tab --name –gc) and sequence identity with respect to the human ortholog using EMBOSS-needle [107].

Squamate lineage-specific evidence of segmental deletion

a. Dataset preparation

We developed an integrated analysis pipeline encompassing orthologue retrieval, synteny mapping, intergenic distance measurement, and gap detection to investigate segmental deletions underlying unretrieved orthologs. Firstly, four neighbouring syntenic genes (two upstream and two downstream of the focal gene) were identified with synteny analysis, and their orthologs across vertebrate genomes were retrieved from NCBI datasets (parameters: --include product-report --ortholog all). The longest isoform was selected for each ortholog based on protein length and species, where orthologs of all four syntenic genes were annotated. We calculated pairwise intergenic distances using BEDTools closest. Gene pairs on different chromosomes were flagged as potential Evolutionary Breakpoint Regions (EBRs). A comprehensive gene distance matrix with complete orthologous information was assembled for all species. Next, to detect gaps in the locus, genomic intervals spanning the outermost flanking genes were merged with BEDTools merge -d 100000000, and the corresponding sequences were retrieved using NCBI efetch. These regions were scanned for assembly gaps using the Klumpy v1.0.10 find_gaps subprogram, and the total number of gaps was recorded per species. Each species' taxonomy classification (class and order) was obtained using NCBI Taxonomy resources (esearch and efetch). Finally, all data—including intergenic distances, gap counts, and taxonomic info—were consolidated into a unified summary table. A subset of species with complete data was used for downstream visualisation (heatmap) and phylogenetic logistic regression analysis. Based on the presence of intact synteny and absence of gaps, species were classified as having either an intact locus (non-squamates) or a potentially deleted locus (squamates).

b. Statistical analysis of gene distance and phylogenetic signal

i. Ratio-Based Comparative Analysis

To evaluate whether changes in intergenic distances between the focal gene (genes which are unretrievable in squamates) and its flanking genes are associated with segmental

deletion, we first excluded species exhibiting large-scale genomic disruptions such as gaps and EBRs. We calculated six pairwise ratios representing the remaining species' upstream, downstream, and across-gene intergenic distances. We conducted Wilcoxon rank-sum tests for each ratio with the alternative hypothesis set to “less” to compare distributions between species with intact versus deleted gene loci. The resulting *p*-values were adjusted for multiple testing using the FDR method, and significant comparisons were visualised as a heatmap using the pheatmap package in R [108].

ii. Phylogenetic Logistic Regression

To quantify the phylogenetic association between relative gene distance and gene loss, we performed phylogenetic logistic regression using the “phylolm” R package [109]. Squamates (0) and non-squamates (1) were used as the binary variable. The independent variable was the relative intergenic distance for the focal gene, computed as:

$$\overleftarrow{G_{L2}} \qquad \overrightarrow{G_{L1}} \qquad \overrightarrow{\overrightarrow{focal\ gene}} \qquad \overleftarrow{G_{R1}} \qquad \overrightarrow{G_{R2}}$$

Where

G_{L1}: Gene on the left flank of a lost gene on 1st position

G_{L2}: Gene on the left flank of a lost gene on 2nd position

G_{R1}: Gene on the right flank of a lost gene on 1^{st}position

G_{R2}: Gene on the right flank of a lost gene on 2^{nd}position

$focal\ gene$: unretrieved orthologs in squamates

The direction of the arrow indicates gene orientation

$$Relative\ distance\ in\ percentage\ = \left(\frac{d_{focal}}{d_{upstream} + d_{focal} + d_{downstream}}\right) \times 100$$

Where

$$d_{focal} = \text{distance between } G_{L1} \text{ and } G_{R1}$$

$$d_{downstream} = \text{distance between } G_{L1} \text{ and } G_{L2}$$

$$d_{upstream} = \text{distance between } G_{R1} \text{ and } G_{R2}$$

Two methods were used for model fitting: logistic_MPLE and logistic_IG10 (Additional file 1: Table S1).

An UpSet plot was used to visualise multiple lines of evidence supporting gene loss, including synteny-based indicators of segmental deletion or chromosomal rearrangement, genome blast coverage, validation of genome assembly integrity at the gene locus using klumpy, phylogenetic analyses for ortholog and paralog detection using whole-genome sequencing data, hybpiper & IQ-TREE, evidence of segmental deletion inferred from intergenic distances, paralog annotations from Ensembl, and orthologous sequence-based metrics such as GC content and sequence identity.

Signatures of receptor-ligand co-evolution as indirect evidence of *IL34* loss in squamates

Structurally similar ligands can functionally compensate for the loss of each other [110]. Therefore, to explore the evolutionary impact of *IL34* loss in squamates, we investigated the *IL34–CSF1–CSF1R* signalling axis, focusing on the functional interplay between these ligands (*IL34*, *CSF1*) and their shared receptor *CSF1R*. *CSF1R* is a type III receptor tyrosine kinase critical for developing, surviving, and functioning myeloid lineage cells [111]. Previous studies have shown evolutionary co-variation between *IL34* and *CSF1R*, but not between *CSF1* and *CSF1R* [Garceau et al. [59] and reviewed in [60]]. Based on this, we hypothesised that *IL34* loss may influence the evolution and function of *CSF1R* in squamates. We leveraged ENSEMBL annotation for *CSF1R* across vertebrates and retrieved the coding DNA sequence (CDS) of the *CSF1R* with a conserved exon phase (Additional file: Table S10). Multiple sequence alignments (MSAs) of intact *CSF1R* from Squamates and vertebrate

clades were generated using PRANK v.170427 in the Guidance2 suite [112, 113]. Nucleotide sequence alignments were trimmed using trimAl v1.4.1 (parameters: *-resoverlap 0.05 -seqoverlap 90*), removing sequences with >10% gaps and positions with gaps in >5% of sequences [114] and used to assess the strength of selection. Further, the alignments and phylogenetic tree obtained from the Timetree website (https://timetree.org/) were used to investigate the strength of selection [58]. We relied on the dN/dS-based method of Hyphy v2.5.48 and PAML v4.9f [115, 116]. Our selection suite consists of RELAX, BUSTED, aBSERL, MEME, and FEL frameworks of branch-site and site models of Hyphy, along with the null (M0) and branch (branch-free and branch-neutral) models of codeml [117–123]. To investigate whether the gene evolves under relaxed selection, we specified one branch as the foreground and all other branches as the background at a time in the RELAX model of the HyPhy program [68] and codeML of the PAML program [69]. A significant result of $k > 1$ indicates intensified selection along test branches, while $k < 1$ suggests relaxed selection, with significance determined at $p < 0.05$. We also implemented aBSREL and BUSTED, which are branch and gene-wide tests, respectively, to test for signatures of selection on branches of the genes. Site-specific models, such as FEL and MEME, were used to identify sites evolving under positive and negative selection, and ggplot2 was used for visualisation in the R program [124].

Quantifying cross-species alignment conservation

To validate the absence of unretrieved orthologs in squamates, we utilised pair-wise genome alignment to quantify the alignment coverage of diverse vertebrates and compared squamates vs non-squamate orders. For this, we analysed pairwise whole-genome alignments between chicken (GRCg7b) and 27 other vertebrate species, including squamates, using precomputed LASTZ alignments from the Ensembl Comparative database (https://ftp.ensembl.org/pub/current_maf/ensembl-compara/pairwise_alignments/) [104].

Additionally, we created seven new pairwise whole genome alignments using newly available squamates genome assemblies with BUSCO > 96% (Additional file 1: Table S12). The multiple alignment format (MAF) files for each species were downloaded and processed using MafFilter v1.3.1 [125] with the OutputCoordinates filter enabled (output_src_size=yes) to extract conserved syntenic blocks between chicken and the focal species. Next, we used BEDTools intersect with the -wao option to compute overlap between each exon of 53 genes and the aligned regions for each focal species. Finally, to assess alignment for each unretrieved ortholog, we normalised the aligned region with CDS length. The resulting matrix (gene × species) of normalised aligned values was visualised as a heatmap using the pheatmaps v1.0.13 R package (Additional file 1: Table S9). Pairwise Wilcoxon rank-sum tests (alternative = "greater") were performed to compare the aligned regions between squamates and other orders. Multiple testing correction was applied using the "BH" method, and adjusted p-values were used to assess significance (Additional file 1: Table S9). Comparisons of alignments across syntenic genes within squamates were visualised using alluvial plots and heatmaps followed by statistical evaluation using Wilcoxon rank-sum tests (alternative = "less") to compare the left and right neighbouring genes of each focal unretrieved ortholog. Genome alignments of squamate species were assessed using both the assemblies available in Ensembl and those generated in this study.

Data availability

The data and relevant code for this study are available on GitHub:
https://github.com/CEGLAB-Buddhabhushan/Missing_genes_in_squamata.git

Abbreviations

EBR: Evolutionary Breakpoint Region

HBV: Hepatitis B Virus

MYA: Million Years Ago

TCR: T Cell Receptor

PacBio: Pacific Biosciences

ONT: Oxford Nanopore Technologies

FDR: False Discovery Rate

BH: Benjamini–Hochberg correction

NCBI: National Center for Biotechnology Information

BLASTn: Basic Local Alignment Search Tool (nucleotide)

MAF: Multiple Alignment Format

IGV: Integrative Genomics Viewer

RNA-seq: RNA sequencing

Mb: Megabase

Kb: Kilobase

References

1. Burssed B, Zamariolli M, Bellucco FT, Melaragno MI. Mechanisms of structural chromosomal rearrangement formation. Mol Cytogenet. 2022;15.

2. Claude SJ, Park S, Park SJ. Gene loss, genome rearrangement, and accelerated substitution rates in plastid genome of Hypericum ascyron (Hypericaceae). BMC Plant Biol. 2022;22.

3. Huang Z, De O. Furo I, Liu J, Peona V, Gomes AJB, Cen W, et al. Recurrent chromosome reshuffling and the evolution of neo-sex chromosomes in parrots. Nat Commun. 2022;13.

4. Harewood L, Fraser P. The impact of chromosomal rearrangements on regulation of gene expression. Hum Mol Genet. 2014;23:R76–82.

5. Stewart NB, Rogers RL. Chromosomal rearrangements as a source of new gene formation in Drosophila yakuba. PLOS Genet. 2019;15:e1008314.

6. Salve BG, Kurian AM, Vijay N. Concurrent loss of ciliary genes WDR93 and CFAP46 in phylogenetically distant birds. R Soc Open Sci. 2023;10.

7. Ungrová L, Geryk J, Kohn M, Kučerová D, Krchlíková V, Hron T, et al. Avian interferon regulatory factor (IRF) family reunion: IRF3 and IRF9 found. BMC Biol. 2025;23:1–19.

8. Stankiewicz P, Shaw CJ, Withers M, Inoue K, Lupski JR. Serial segmental duplications during primate evolution result in complex human genome architecture. Genome Res. 2004;14:2209–20.

9. Hinsch H, Hannenhalli S. Recurring genomic breaks in independent lineages support genomic fragility. BMC Evol Biol. 2006;6:1–12.

10. Emanuel BS, Shaikh TH. Segmental duplications: an “expanding” role in genomic instability and disease. Nat Rev Genet. 2001;2:791–800.

11. Shinde SS, Sharma S, Teekas L, Sharma A, Vijay N. Recurrent erosion of COA1/MITRAC15 exemplifies conditional gene dispensability in oxidative phosphorylation. Sci Reports 2021 111. 2021;11:1–16.

12. Meredith RW, Gatesy J, Cheng J, Springer MS. Pseudogenization of the tooth gene enamelysin (MMP20) in the common ancestor of extant baleen whales. Proc R Soc B Biol Sci. 2011;278:993–1002.

13. Albalat R, Cañestro C. Evolution by gene loss. Nat Rev Genet 2016 177. 2016;17:379–91.

14. Blumer M, Brown T, Freitas MB, Destro AL, Oliveira JA, Morales AE, et al. Gene losses in the common vampire bat illuminate molecular adaptations to blood feeding. Sci Adv. 2022;8:6494.

15. Sharma V, Hecker N, Roscito JG, Foerster L, Langer BE, Hiller M. A genomics approach reveals insights into the importance of gene losses for mammalian adaptations. Nat Commun 2018 91. 2018;9:1–9.

16. Guijarro-Clarke C, Holland PWH, Paps J. Widespread patterns of gene loss in the evolution of the animal kingdom. Nat Ecol Evol 2020 44. 2020;4:519–23.

17. Koepfli KP, Paten B, O’brien SJ, Antunes A, Belov K, Bustamante C, et al. The Genome 10K Project: a way forward. Annu Rev Anim Biosci. 2015;3:57–111.

18. Jarvis ED, Mirarab S, Aberer AJ, Li B, Houde P, Li C, et al. Phylogenomic analyses data of the avian phylogenomics project. Gigascience. 2015;4.

19. Jebb D, Huang Z, Pippel M, Hughes GM, Lavrichenko K, Devanna P, et al. Six reference-quality genomes reveal evolution of bat adaptations. Nature. 2020;583:578–84.

20. Stiller J, Feng S, Chowdhury AA, Rivas-González I, Duchêne DA, Fang Q, et al. Complexity of avian evolution revealed by family-level genomes. Nat 2024 6298013. 2024;629:851–60.

21. Wheeler DL, Barrett T, Benson DA, Bryant SH, Canese K, Chetvernin V, et al. Database resources of the National Center for Biotechnology Information. Nucleic Acids Res. 2007;35 SUPPL. 1.

22. Rangwala SH, Kuznetsov A, Ananiev V, Asztalos A, Borodin E, Evgeniev V, et al. Accessing NCBI data using the NCBI Sequence Viewer and Genome Data Viewer (GDV). Genome Res. 2021;31:159–69.

23. Friocourt F, Lafont AG, Kress C, Pain B, Manceau M, Dufour S, et al. Recurrent DCC

gene losses during bird evolution. Sci Reports 2017 71. 2017;7:1–11.

24. Kato A, Pipil S, Ota C, Kusakabe M, Watanabe T, Nagashima A, et al. Convergent gene losses and pseudogenizations in multiple lineages of stomachless fishes. Commun Biol. 2024;7:408.

25. Simões TR, Caldwell MW, Tałanda M, Bernardi M, Palci A, Vernygora O, et al. The origin of squamates revealed by a Middle Triassic lizard from the Italian Alps. Nature. 2018;557:706–9.

26. Gemmell NJ, Rutherford K, Prost S, Tollis M, Winter D, Macey JR, et al. The tuatara genome reveals ancient features of amniote evolution. Nat 2020 5847821. 2020;584:403–9.

27. Simões TR, Pyron RA. THE SQUAMATE TREE OF LIFE. Bull Museum Comp Zool. 2021;163:47–95.

28. Mezzasalma M, Macirella R, Odierna G, Brunelli E. Karyotype Diversification and Chromosome Rearrangements in Squamate Reptiles. Genes 2024, Vol 15, Page 371. 2024;15:371.

29. Waters PD, Patel HR, Ruiz-Herrera A, Alvarez-Gonzalez L, Lister NC, Simakov O, et al. Microchromosomes are building blocks of bird, reptile, and mammal chromosomes. Proc Natl Acad Sci U S A. 2021;118:e2112494118.

30. Pinto BJ, Gamble T, Smith CH, Wilson MA. A lizard is never late: Squamate genomics as a recent catalyst for understanding sex chromosome and microchromosome evolution. J Hered. 2023;114:445–58.

31. Emerling CA. Genomic regression of claw keratin, taste receptor and light-associated genes provides insights into biology and evolutionary origins of snakes. Mol Phylogenet Evol. 2017;115:40–9.

32. Roscito JG, Sameith K, Kirilenko BM, Hecker N, Winkler S, Dahl A, et al. Convergent and lineage-specific genomic differences in limb regulatory elements in limbless reptile lineages. Cell Rep. 2022;38:110280.

33. Gable SM, Mendez JM, Bushroe NA, Wilson A, Byars MI, Tollis M. The State of Squamate Genomics: Past, Present, and Future of Genome Research in the Most Speciose Terrestrial Vertebrate Order. Genes (Basel). 2023;14:1387.

34. Modi WS, Crews D. Sex chromosomes and sex determination in reptiles: Commentary. Curr Opin Genet Dev. 2005;15:660–5.

35. Gable SM, Bushroe NA, Mendez JM, Wilson A, Pinto BJ, Gamble T, et al. Differential Conservation and Loss of Chicken Repeat 1 (CR1) Retrotransposons in Squamates Reveal Lineage-Specific Genome Dynamics Across Reptiles. Genome Biol Evol. 2024;16.

36. Alföldi J, Di Palma F, Grabherr M, Williams C, Kong L, Mauceli E, et al. The genome of the green anole lizard and a comparative analysis with birds and mammals. Nature. 2011;477:587–91.

37. Kapusta A, Suh A, Feschotte C. Dynamics of genome size evolution in birds and mammals. Proc Natl Acad Sci U S A. 2017;114:E1460–9.

38. Lovell P V, Wirthlin M, Wilhelm L, Minx P, Lazar NH, Carbone L, et al. Conserved syntenic clusters of protein coding genes are missing in birds. Genome Biol. 2014;15:565.

39. Olson M V. When Less Is More: Gene Loss as an Engine of Evolutionary Change. Am J Hum Genet. 1999;64:18–23.

40. Sánchez-Serna G, Badia-Ramentol J, Bujosa P, Ferrández-Roldán A, Torres-Águila NP, Fabregà-Torrus M, et al. Less, but More: New Insights From Appendicularians on Chordate Fgf Evolution and the Divergence of Tunicate Lifestyles. Mol Biol Evol. 2025;42.

41. Hoffmann FG, Opazo JC, Storz JF. Whole-Genome Duplications Spurred the Functional Diversification of the Globin Gene Superfamily in Vertebrates. Mol Biol Evol. 2012;29:303–12.

42. Kim J, Lee C, Ko BJ, Yoo DA, Won S, Phillippy AM, et al. False gene and chromosome losses in genome assemblies caused by GC content variation and repeats. Genome Biol. 2022;23:1–29.

43. Rhie A, McCarthy SA, Fedrigo O, Damas J, Formenti G, Koren S, et al. Towards complete and error-free genome assemblies of all vertebrate species. 2021;592:737–46.

44. Zhou Y, Shearwin-Whyatt L, Li J, Song Z, Hayakawa T, Stevens D, et al. Platypus and echidna genomes reveal mammalian biology and evolution. Nat 2020 5927856. 2021;592:756–62.

45. Gould SJ. Is uniformitarianism necessary? Am J Sci. 1965;263:223–8.

46. Drabeck DH, Wiese J, Gilbertson E, Arroyave J, Stiassny MLJ, Alter SE, et al. Gene loss and relaxed selection of plaat1 in vertebrates adapted to low-light environments. Proc R Soc B. 2024;291.

47. Gower DJ, Fleming JF, Pisani D, Vonk FJ, Kerkkamp HMI, Peichl L, et al. Eye-Transcriptome and Genome-Wide Sequencing for Scolecophidia: Implications for Inferring the Visual System of the Ancestral Snake. Genome Biol Evol. 2021;13.

48. Pinheiro D, Mawhin MA, Prendecki M, Woollard KJ. In-silico analysis of myeloid cells across the animal kingdom reveals neutrophil evolution by colony-stimulating factors. Elife. 2020;9:1–20.

49. Hron T, Pajer P, Pačes J, Bartůněk P, Elleder D. Hidden genes in birds. Genome Biol. 2015;16:164.

50. Bornelöv S, Seroussi E, Yosefi S, Pendavis K, Burgess SC, Grabherr M, et al. Correspondence on Lovell et al.: identification of chicken genes previously assumed to be evolutionarily lost. Genome Biol. 2017;18:112.

51. Hara Y, Kuraku S. The impact of local genomic properties on the evolutionary fate of genes. Elife. 2023;12.

52. Rohde F, Schusser B, Hron T, Farkašová H, Plachý J, Härtle S, et al. Characterization of chicken tumor necrosis factor-α, a long missed cytokine in birds. Front Immunol. 2018;9 APR:605.

53. Janusova S, Krchlikova V, Hron T, Elleder D, Stepanek O. Identification of GC-rich LAT genes in birds. PLoS One. 2023;18 4 April:11–4.

54. Salve BG, Sharma S, Vijay N. Evolutionary diversity of CXCL16-CXCR6: Convergent substitutions and recurrent gene loss in sauropsids. Immunogenet 2024 765. 2024;76:397–415.

55. Brocker C, Thompson D, Matsumoto A, Nebert DW, Vasiliou V. Evolutionary divergence and functions of the human interleukin (IL) gene family. Hum Genomics. 2010;5:30.

56. Nei M, Gu X, Sitnikova T. Evolution by the birth-and-death process in multigene families of the vertebrate immune system. Proc Natl Acad Sci U S A. 1997;94:7799–806.

57. Nei M, Rooney AP. Concerted and birth-and-death evolution of multigene families. Annu Rev Genet. 2005;39 Volume 39, 2005:121–52.

58. Kumar S, Stecher G, Suleski M, Hedges SB. TimeTree: A Resource for Timelines, Timetrees, and Divergence Times. Mol Biol Evol. 2017;34:1812–9.

59. Garceau V, Smith J, Paton IR, Davey M, Fares MA, Sester DP, et al. Pivotal Advance: Avian colony-stimulating factor 1 (CSF-1), interleukin-34 (IL-34), and CSF-1 receptor genes and gene products. J Leukoc Biol. 2010;87:753–64.

60. Baghdadi M, Umeyama Y, Hama N, Kobayashi T, Han N, Wada H, et al. Interleukin-34, a comprehensive review. J Leukoc Biol. 2018;104:931–51.

61. Ko BJ, Lee C, Kim J, Rhie A, Yoo DA, Howe K, et al. Widespread false gene gains caused by duplication errors in genome assemblies. Genome Biol. 2022;23:1–26.

62. Hume DA, Gutowska-Ding MW, Garcia-Morales C, Kebede A, Bamidele O, Trujillo AV, et al. Functional evolution of the colony-stimulating factor 1 receptor (CSF1R) and its ligands in birds. J Leukoc Biol. 2020;107:237–50.

63. Bayly-Jones C, Whisstock JC. Mining folded proteomes in the era of accurate structure prediction. PLOS Comput Biol. 2022;18:e1009930.

64. Deem KD, Brisson JA. Problems with Paralogs: The Promise and Challenges of Gene Duplicates in Evo-Devo Research. Integr Comp Biol. 2024;64:556.

65. Neves F, Marques JP, Areal H, Pinto-Pinho P, Colaço B, Melo-Ferreira J, et al. TLR7 and TLR8 evolution in lagomorphs: different patterns in the different lineages. Immunogenetics. 2022;74:475–85.

66. Baird DM. Telomeres and genomic evolution. Philos Trans R Soc B Biol Sci. 2018;373.

67. Sedlazeck FJ, Lee H, Darby CA, Schatz MC. Piercing the dark matter: bioinformatics of long-range sequencing and mapping. Nat Rev Genet 2018 196. 2018;19:329–46.

68. Li M, Sun C, Xu N, Bian P, Tian X, Wang X, et al. De Novo Assembly of 20 Chicken Genomes Reveals the Undetectable Phenomenon for Thousands of Core Genes on Microchromosomes and Subtelomeric Regions. Mol Biol Evol. 2022;39.

69. Seroussi E, Cinnamon Y, Yosefi S, Genin O, Smith JG, Rafati N, et al. Identification of the Long-Sought Leptin in Chicken and Duck: Expression Pattern of the Highly GC-Rich Avian leptin Fits an Autocrine/Paracrine Rather Than Endocrine Function. Endocrinology. 2016;157:737–51.

70. Neves F, Abrantes J, Steinke JW, Esteves PJ. Maximum-likelihood approaches reveal signatures of positive selection in IL genes in mammals. Innate Immun. 2014;20:184–91.

71. Neves F, Abrantes J, Almeida T, De Matos AL, Costa PP, Esteves PJ. Genetic characterization of interleukins (IL-1α, IL-1β, IL-2, IL-4, IL-8, IL-10, IL-12A, IL-12B, IL-15 and IL-18) with relevant biological roles in lagomorphs. Innate Immun. 2015;21:787–801.

72. Sironi M, Cagliani R, Forni D, Clerici M. Evolutionary insights into host-pathogen interactions from mammalian sequence data. Nat Rev Genet. 2015;16:224–36.

73. Tenthorey JL, Emerman M, Malik HS. Evolutionary Landscapes of Host-Virus Arms Races. Annu Rev Immunol. 2022;40 Volume 40, 2022:271–94.

74. Wang X, Grus WE, Zhang J. Gene Losses during Human Origins. PLOS Biol. 2006;4:e52.

75. Helsen J, Voordeckers K, Vanderwaeren L, Santermans T, Tsontaki M, Verstrepen KJ, et al. Gene Loss Predictably Drives Evolutionary Adaptation. Mol Biol Evol. 2020;37:2989–3002.

76. Brandis G, Hughes D. The SNAP hypothesis: Chromosomal rearrangements could emerge from positive Selection during Niche Adaptation. PLoS Genet. 2020;16.

77. van der Loo W, Magalhaes MJ, de Matos AL, Abrantes J, Yamada F, Esteves PJ. Adaptive Gene Loss? Tracing Back the Pseudogenization of the Rabbit CCL8 Chemokine. J Mol Evol. 2016;83:12–25.

78. Baghdadi M, Endo H, Tanaka Y, Wada H, Seino K ichiro. Interleukin 34, from pathogenesis to clinical applications. Cytokine. 2017;99:139–47.

79. Walker DG, Tang TM, Lue LF. Studies on colony stimulating factor receptor-1 and ligands colony stimulating factor-1 and interleukin-34 in Alzheimer's disease brains and human microglia. Front Aging Neurosci. 2017;9 AUG:271250.

80. Cheng ST, Tang H, Ren JH, Chen X, Huang AL, Chen J. Interleukin-34 inhibits hepatitis B virus replication in vitro and in vivo. PLoS One. 2017;12:e0179605.

81. Hossainey MRH, Hauser KA, Garvey CN, Kalia N, Garvey JM, Grayfer L. A perspective into the relationships between amphibian (Xenopus laevis) myeloid cell subsets. Philos Trans R Soc B Biol Sci. 2023;378.

82. Lopez Ruiz V, Robert J. The amphibian immune system. Philos Trans R Soc B. 2023;378.

83. Lin H, Lee E, Hestir K, Leo C, Huang M, Bosch E, et al. Discovery of a Cytokine and Its Receptor by Functional Screening of the Extracellular Proteome. Science (80-). 2008;320:807–11.

84. Wang Y, Szretter KJ, Vermi W, Gilfillan S, Rossini C, Cella M, et al. IL-34 is a tissue-restricted ligand of CSF1R required for the development of Langerhans cells and microglia. Nat Immunol. 2012;13:753–60.

85. Greter M, Lelios I, Pelczar P, Hoeffel G, Price J, Leboeuf M, et al. Stroma-Derived Interleukin-34 Controls the Development and Maintenance of Langerhans Cells and the Maintenance of Microglia. Immunity. 2012;37:1050–60.

86. Kagohashi K, Sasaki Y, Ozawa K, Tsuchiya T, Kawahara S, Saitoh K, et al. Role of Signal-Transducing Adaptor Protein-1 for T Cell Activation and Pathogenesis of Autoimmune Demyelination and Airway Inflammation. J Immunol. 2024;212:951–61.

87. Banks CAS, Boanca G, Lee ZT, Eubanks CG, Hattem GL, Peak A, et al. TNIP2 is a Hub Protein in the NF-κB Network with Both Protein and RNA Mediated Interactions. Mol Cell Proteomics. 2016;15:3435–49.

88. Van Huffel S, Delaei F, Heyninck K, De Valck D, Beyaert R. Identification of a Novel A20-binding Inhibitor of Nuclear Factor-κB Activation Termed ABIN-2. J Biol Chem. 2001;276:30216–23.

89. Zhao L, Wang S, Xu M, He Y, Zhang X, Xiong Y, et al. Vpr counteracts the restriction of LAPTM5 to promote HIV-1 infection in macrophages. Nat Commun 2021 121. 2021;12:1–14.

90. O'Leary NA, Cox E, Holmes JB, Anderson WR, Falk R, Hem V, et al. Exploring and retrieving sequence and metadata for species across the tree of life with NCBI Datasets. Sci Data 2024 111. 2024;11:1–10.

91. Lovell JT, Sreedasyam A, Schranz ME, Wilson M, Carlson JW, Harkess A, et al. GENESPACE tracks regions of interest and gene copy number variation across multiple genomes. Elife. 2022;11.

92. Cer RZ, Donohue DE, Mudunuri US, Temiz NA, Loss MA, Starner NJ, et al. Non-B DB v2.0: A database of predicted non-B DNA-forming motifs and its associated tools. Nucleic Acids Res. 2013;41.

93. Rangwala SH, Rudnev D V., Ananiev V V., Oh DH, Asztalos A, Benica B, et al. The NCBI Comparative Genome Viewer (CGV) is an interactive visualization tool for the analysis of whole-genome eukaryotic alignments. PLOS Biol. 2024;22:e3002405.

94. Altschul SF, Gish W, Miller W, Myers EW, Lipman DJ. Basic local alignment search tool. J Mol Biol. 1990;215:403–10.

95. Robinson JT, Thorvaldsdottir H, Turner D, Mesirov JP. igv.js: an embeddable JavaScript implementation of the Integrative Genomics Viewer (IGV). Bioinformatics. 2023;39.

96. Johnson MG, Gardner EM, Liu Y, Medina R, Goffinet B, Shaw AJ, et al. HybPiper: Extracting coding sequence and introns for phylogenetics from high-throughput sequencing reads using target enrichment. Appl Plant Sci. 2016;4.

97. Minh BQ, Schmidt HA, Chernomor O, Schrempf D, Woodhams MD, Von Haeseler A, et al. IQ-TREE 2: New Models and Efficient Methods for Phylogenetic Inference in the Genomic Era. Mol Biol Evol. 2020;37:1530–4.

98. Paradis E, Blomberg S, Bolker B, Brown J, Claramunt S, Claude J, et al. Analyses of Phylogenetics and Evolution [R package ape version 5.8-1]. CRAN Contrib Packag. 2024. https://doi.org/10.32614/CRAN.PACKAGE.APE.

99. Guo Q, Pan Y, Dai W, Guo F, Zeng T, Chen W, et al. A near-complete genome assembly of the bearded dragon Pogona vitticeps provides insights into the origin of Pogona sex chromosomes. Gigascience. 2025;14.

100. Patel HR, Alreja K, Reis ALM, Chang JK, Chew ZA, Jung H, et al. A near telomere-to-telomere phased genome assembly and annotation for the Australian central bearded dragon Pogona vitticeps. Gigascience. 2025;14.

101. Emms DM, Kelly S. OrthoFinder: Phylogenetic orthology inference for comparative genomics. Genome Biol. 2019;20:1–14.

102. Li H. Minimap2: pairwise alignment for nucleotide sequences. Bioinformatics. 2018;34:3094–100.

103. Tang AD, Soulette CM, van Baren MJ, Hart K, Hrabeta-Robinson E, Wu CJ, et al. Full-length transcript characterization of SF3B1 mutation in chronic lymphocytic leukemia reveals downregulation of retained introns. Nat Commun. 2020;11.

104. Martin FJ, Amode MR, Aneja A, Austine-Orimoloye O, Azov AG, Barnes I, et al. Ensembl 2023. Nucleic Acids Res. 2023;51:D933–41.

105. Madrigal G, Minhas BF, Catchen J. Klumpy: A tool to evaluate the integrity of long-read genome assemblies and illusive sequence motifs. Mol Ecol Resour. 2024;:e13982.

106. Beauclair L, Ramé C, Arensburger P, Piégu B, Guillou F, Dupont J, et al. Sequence properties of certain GC rich avian genes, their origins and absence from genome assemblies: Case studies. BMC Genomics. 2019;20:734.

107. Rice P, Longden L, Bleasby A. EMBOSS: The European Molecular Biology Open Software Suite. Trends Genet. 2000;16:276–7.

108. Kolde R. pheatmap: Pretty Heatmaps. CRAN Contrib Packag. 2010. https://doi.org/10.32614/CRAN.PACKAGE.PHEATMAP.

109. Ives AR, Garland T. Phylogenetic Logistic Regression for Binary Dependent Variables. Syst Biol. 2010;59:9–26.

110. Krchlíková V, Hron T, Těšický M, Li T, Ungrová L, Hejnar J, et al. Dynamic Evolution of Avian RNA Virus Sensors: Repeated Loss of RIG-I and RIPLET. Viruses. 2023;15.

111. Stanley ER, Chitu V. CSF-1 receptor signaling in myeloid cells. Cold Spring Harb Perspect Biol. 2014;6.

112. Sela I, Ashkenazy H, Katoh K, acids research TP-N, undefined 2015. GUIDANCE2: accurate detection of unreliable alignment regions accounting for the uncertainty of multiple parameters. academic.oup.com. 2015;43:7–14.

113. Löytynoja A. Phylogeny-aware alignment with PRANK. Methods Mol Biol. 2014;1079:155–70.

114. Capella-Gutiérrez S, Silla-Martínez JM, Gabaldón T. trimAl: a tool for automated alignment trimming in large-scale phylogenetic analyses. Bioinformatics. 2009;25:1972–3.

115. Kosakovsky Pond SL, Frost SDW, Muse S V. HyPhy: Hypothesis testing using phylogenies. Bioinformatics. 2005.

116. Yang Z. PAML 4: Phylogenetic Analysis by Maximum Likelihood. Mol Biol Evol. 2007;24:1586–91.

117. Smith MD, Wertheim JO, Weaver S, Murrell B, Scheffler K, Kosakovsky Pond SL. Less is more: an adaptive branch-site random effects model for efficient detection of episodic diversifying selection. Mol Biol Evol. 2015;32:1342–53.

118. Murrell B, Weaver S, Smith MD, Wertheim JO, Murrell S, Aylward A, et al. Gene-wide identification of episodic selection. Mol Biol Evol. 2015;32:1365–71.

119. Kosakovsky Pond SL, Frost SDW. Not so different after all: A comparison of methods for detecting amino acid sites under selection. Mol Biol Evol. 2005;22:1208–22.

120. Murrell B, Wertheim JO, Moola S, Weighill T, Scheffler K, Kosakovsky Pond SL. Detecting Individual Sites Subject to Episodic Diversifying Selection. PLOS Genet.

2012;8:e1002764.

121. Wertheim JO, Murrell B, Smith MD, Kosakovsky Pond SL, Scheffler K. RELAX: Detecting Relaxed Selection in a Phylogenetic Framework. Mol Biol Evol. 2015;32:820–32.

122. Poon AFY, Lewis FI, Kosakovsky Pond SL, Frost SDW. An Evolutionary-Network Model Reveals Stratified Interactions in the V3 Loop of the HIV-1 Envelope. PLOS Comput Biol. 2007;3:e231.

123. Yang Z, Nielsent R. Codon-Substitution Models for Detecting Molecular Adaptation at Individual Sites Along Specific Lineages. Mol Biol Evol. 2002;19:908–17.

124. Wickham H. ggplot2. 2016. https://doi.org/10.1007/978-3-319-24277-4.

125. Dutheil JY, Gaillard S, Stukenbrock EH. MafFilter: A highly flexible and extensible multiple genome alignment files processor. BMC Genomics. 2014;15:1–10.

Acknowledgements

We gratefully acknowledge the Vertebrate Genomes Project (VGP; https://vertebrategenomesproject.org) for generating and making available the high-quality genome assemblies that greatly facilitated this work. We thank the Council of Scientific & Industrial Research (CSIR) and the University Grant Commission (UGC) for a fellowship to BGS and SH, respectively. We used BioRender (https://biorender.com) to arrange figures and images of species.

Funding

This article was funded by the Department of Biotechnology, Ministry of Science and Technology, India (grant no. BT/11/IYBA/2018/03) and Science and Engineering Research Board (grant no. ECR/2017/001430) provided funds for procuring computational resources (i.e. Har Gobind Khorana Computational Biology cluster) used.

Author information

Authors and Affiliations

Buddhabhushan Girish Salve (buddhabhushan21@iiserb.ac.in), Sonal H (sonal24@iiserb.ac.in), Nagarjun Vijay (nagarjun@iiserb.ac.in)

Computational Evolutionary Genomics Lab, Department of Biological Sciences, IISER Bhopal, Bhauri, Madhya Pradesh, India

Contributions

BGS and NV. conceived and designed the study; BGS, SH, and NV performed research and analysed data; and BGS, SH and NV wrote the manuscript. All authors have read and approved the final version of the manuscript and agree with the order of presentation of the authors.

Corresponding author

Correspondence to Nagarjun Vijay (nagarjun@iiserb.ac.in)

Ethics declarations

Ethics approval and consent to participate

Not applicable.

Consent for publication

Not applicable.

Competing interests

The authors declare no competing interests.

Figure legends

Fig. 1

Unretrieved orthologs are localised to discrete chromosomal regions, occur within syntenic blocks, and are associated with chromosomal rearrangements. The left panel shows the genomic locations of 53 unretrieved orthologs mapped across 21 chromosomes of the Chicken karyotype (black horizontal bars scaled by genomic position on the x-axis, and chromosome numbers are shown on the left side). Unretrieved orthologs are indicated by light green dots labelled with gene names. GC content, calculated in 100 bp windows, is

represented by a gradient from light grey (low GC) to red (high GC). Below the GC track, the presence of predicted non-B DNA motifs is indicated by colour-coded bars. The right panel depicts chromosomal rearrangements across representative sauropsid species (*Gallus gallus*, *Alligator mississippiensis*, *Chelonia mydas*, *Pogona vitticeps*, *Anolis sagrei*, and *Thamnophis elegans).* The chromosome numbers are mentioned above each grey-coloured rectangle, and coloured ribbons (as defined in the left panel) represent conserved synteny blocks connecting orthologous regions, with seven regions of interest (ROI_1 to ROI_7) highlighted. These regions are implicated in the loss of two or more genes**.** The chicken orthologues of the human genes *IFTAP*, *PLAAT1*, and *TMEM273* correspond to *C11orf74*, *HRASLS*, and *C10orf128*, respectively.

Fig. 2

Multiple lines of evidence support gene loss in the Squamate lineage. **A.** Evidence types used to validate candidate gene losses/unretrieved orthologs. The left panels summarise evidence of segmental deletions (n = 36 genes) and chromosomal rearrangements (n = 17 genes). Upset plots display intersections of evidence categories, including synteny, genome blast coverage, GC content, sequence identity, paralog status (Ensembl), closest paralog placement (Hybpiper and IQ-TREE-based phylogenetic analysis), phylogenetic signal for segmental deletion, intergenic distance-based evidence of segmental deletion, and assembly gaps found using klumpy. Horizontal bar plots show total set size for each evidence type, while vertical bars represent intersection sizes and gene names are mentioned on bars (the font size varies with increase in evidence). The stacked bar plots below indicate cumulative evidence scores for each gene, with contributions color-coded by evidence type. **B.** Quantitative evaluation of evidence metrics across 53 candidate gene losses/unretrieved orthologs. Violin plots display distributions of (i) maximum genome coverage obtained using BLASTn search for each squamate genome, (ii) sequence identity (%), (iii) GC content (%), and (iv) GC stretches.

Each gene is represented by its own distribution profile, with dashed lines marking thresholds used to support gene classification as candidate gene losses or unretrieved orthologs.

Fig. 3

Unretrieved orthologs often belong to multi-gene families of paralogues. Human genes corresponding to squamate- unretrieved orthologs are plotted based on their GC-content (x-axis) and paralogs (y-axis) as annotated in Ensembl. Each point represents a paralogue, with the size of the light-coloured filled circle indicating the percentage sequence identity between the unretrieved orthologs and their paralog. Dashed lines indicate an approximate GC content of 55% for both axes (vertical red for the unretrieved orthologs and horizontal blue for the paralogues). This representation highlights that genes lost in squamates often belong to multi-gene families with moderate GC content.

Fig. 4

LASTZ alignment-based evidence for candidate gene loss in squamates. **A.** Heatmap of normalised aligned regions at the exonic region of Chicken (alignment length/CDS length) for 53 genes across 34 amniote species. Squamates show consistently reduced alignment at focal loci compared to other clades. In some cases, where alignment is detected, it may originate from paralogous sequences rather than true orthologs, while unaligned regions may reflect highly divergent orthologs. **B.** Boxplots of normalised aligned regions across clades for left, focal, and right gene positions. Significant reductions (wilcox.test; alternative = "greater") are observed at focal loci in squamates, which is not the case for other orders. **C.** Comparison of Ensembl LASTZ chains (n = 7 species) and manually created LASTZ chains in this study (n = 6 species with two genomes of *Pogona vitticeps*, of squamate species BUSCO >97) shows no significant difference (Wilcoxon test, p = 0.16). **D.** Clade-level comparison highlights significantly lower alignment coverage in squamates relative to birds,

crocodilians, testudines, and other lineages (wilcox.test; alternative = "greater"). Statistically significant pairwise differences are indicated by bars above the boxplots (*□p□≤□0.05, **□p□≤□0.01, ***□p□≤□0.001, ****□p□≤□0.0001, ns□=□non-significant). Boxplots are generated using ggplot [124].

Fig. 5

Evidence for *IL34* gene loss via segmental deletion. **A.** Micro-gene synteny of *IL34* in 24 vertebrate representative species. The phylogenetic branches of species with *IL34* lost are depicted with dashed red, while blue phylogenetic branches represent the 3rd round of whole genome duplication. The green-coloured thunderbolt marks the gene loss event in squamates. Arrows represent genes, with their direction indicating gene orientation and gene names labelled inside each arrow. **B.** The heatmap shows the reduction in gene distance at the *IL34* locus (between *SF3B3-MTSS2*) in squamates. The values inside the box represent adjusted p-values (significant differences between squamates and non-squamates, calculated using pairwise Wilcox one-tailed test (alternative = “less”). **C.** Phylogenetic logistic regression analyses. The relative genomic distance between flanking genes (x-axis, in %) and the status of the *IL34* gene (y-axis) are correlated using two methods (logistic_IG10 and logistic_MPLE) to evaluate the segmental deletion of the *IL34* gene across vertebrates (n□=□179). The species tree was obtained from the Timetree website (https://timetree.org/) and annotated in iTOL (https://itol.embl.de/). Species images are from https://BioRender.com.

Fig. 6

Validation of genome assembly at *IL34* gene syntenic locus in common wall lizard and Indian cobra genomes using long-read sequencing. UCSC Genome Browser snapshots of the *IL34* syntenic region are shown for the common wall lizard (*Podarcis muralis*; panel A,

chr8:39,120,000–39,125,000) and the Indian cobra (*Naja naja*; panel B, chr4:770,000–780,000). The top portion of each panel displays GC content (black line), annotated syntenic genes (*MTSS2*/*SF3B3* in *P. muralis*, E2320_000953/958 in *N. naja*), and RepeatMasker annotations (including SINEs, LINEs, and low-complexity elements). The bottom portion of both panels shows long-reads from PacBio and Nanopore spanning the entire region. Grey and yellow segments indicate forward- and reverse-strand alignments, respectively. Transparent red and blue boxes mark exons of flanking syntenic genes. SRA (Short Read Archive) accession numbers for the datasets used to generate the BAM files are indicated next to the plots.

Fig. 7

Indirect evidence for *IL34* loss: Co-evolution of receptor *CSF1R*. Selection analysis of the *CSF1R* coding sequence was conducted across 32 vertebrate species using both branch-based (RELAX, aBSREL, and CodeML) and site (FEL and MEME) models. The phylogenetic tree (left) illustrates the evolutionary relationships among species, with squamate lineages highlighted in red text and red box. Selection inferences such as relaxed/intensified and positive selection, based on RELAX, CodeML, and aBSREL analyses, are shown for each species. The central panel displays the distribution of positively and negatively selected codon sites along the gene, with codon positions on the x-axis and selection signals from focal species (foreground) against the rest of the species in the background. The right panel summarises the number of positively selected sites detected by FEL and MEME for each species, visualised using ggplot2 [124].

Fig. 8

Evolutionary relationships and genomic context of caveolin (CAV) genes in Squamates. (A) Maximum-likelihood phylogeny of *CAV1*, *CAV2*, *CAV3*, and *CAV3*-like genes across representative vertebrates. *CAV1* and *CAV2* form distinct clades, while *CAV3* and *CAV3*-like (blue branch) sequences cluster separately. The phylogenetic tree made using IQ-TREE and rooted to *CAV2*. The bootstrap support values are indicated at nodes. (B) Synteny of the *CAV3*-like locus in Pogona vitticeps. (C) Transcriptomic evidence for the *CAV3*-like gene in central bearded dragon (*Pogona vitticeps*). Long-read (Nanopore) and short-read RNA-seq data confirm exon–intron structure and transcriptionally active status of *CAV3*-like (*LOC110078681*) gene in *Pogona vitticeps*.

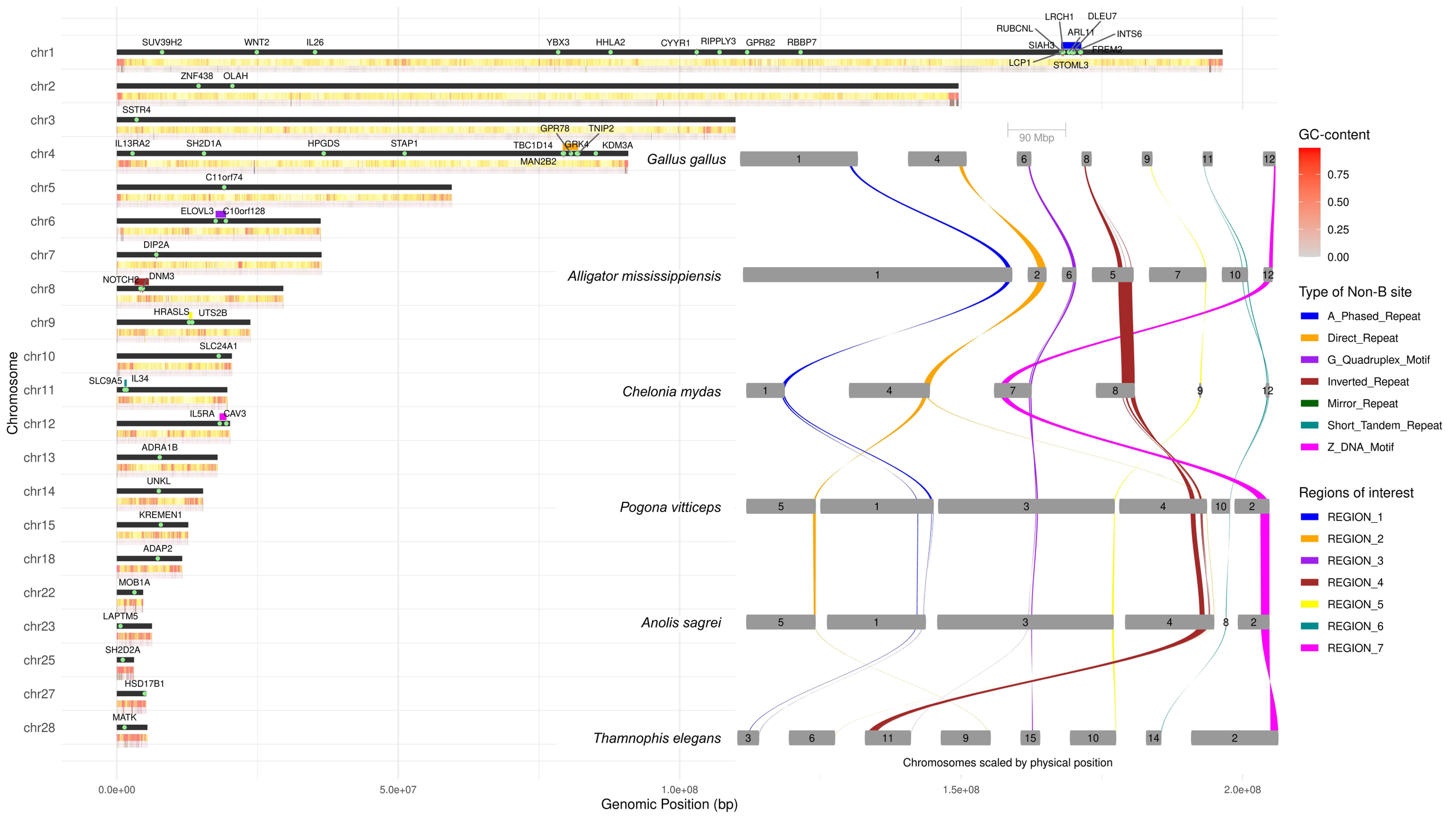
Chromosome
chr1
chr2
chr3
chr4
chr5
chr6
chr7
chr8
chr9
chr10
chr11
chr12
chr13
chr14
chr15
chr18
chr22
chr23
chr25
chr27
chr28
SUV39H2
WNT2
IL26
YBX3
HHLA2
CYYR1
RIPPLY3
GPR82
RBBP7
LRCH1
DLEU7
RUBCNL
ARL11
INTS6
SIAH3
FREM2
LCP1
STOML3
ZNF438
OLAH
SSTR4
GPR78
TNIP2
IL13RA2
SH2D1A
HPGDS
STAP1
TBC1D14
GRK4
KDM3A
MAN2B2
C11orf74
ELOVL3
C10orf128
DIP2A
NOTCH2
DNM3
HRASLS
UTS2B
SLC24A1
SLC9A5
IL34
IL5RA
CAV3
ADRA1B
UNKL
KREMEN1
ADAP2
MOB1A
LAPTM5
SH2D2A
HSD17B1
MATK
0.0e+00
5.0e+07
1.0e+08
1.5e+08
2.0e+08
Genomic Position (bp)
90 Mbp
Gallus gallus
Alligator mississippiensis
Chelonia mydas
Pogona vitticeps
Anolis sagrei
Thamnophis elegans
Chromosomes scaled by physical position
GC-content
0.75
0.50
0.25
0.00
Type of Non-B site
A_Phased_Repeat
Direct_Repeat
G_Quadruplex_Motif
Inverted_Repeat
Mirror_Repeat
Short_Tandem_Repeat
Z_DNA_Motif
Regions of interest
REGION_1
REGION_2
REGION_3
REGION_4
REGION_5
REGION_6
REGION_7

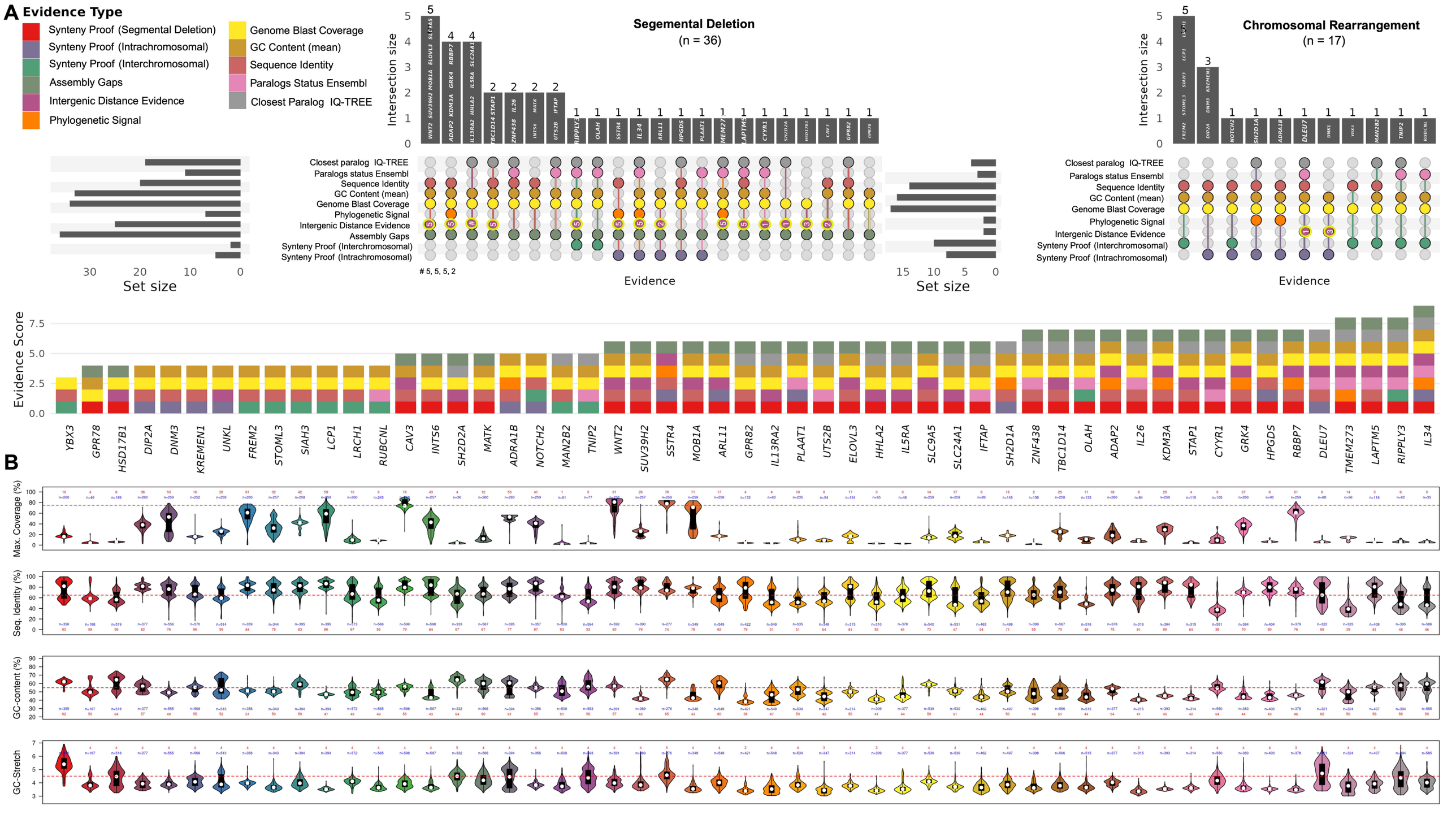
A
Evidence Type
Synteny Proof (Segmental Deletion)
Synteny Proof (Intrachromosomal)
Synteny Proof (Interchromosomal)
Assembly Gaps
Intergenic Distance Evidence
Phylogenetic Signal
Genome Blast Coverage
GC Content (mean)
Sequence Identity
Paralogs Status Ensembl
Closest Paralog IQ-TREE
Segemental Deletion
(n = 36)
Intersection size
Chromosomal Rearrangement
(n = 17)
Closest paralog IQ-TREE
Paralogs status Ensembl
Sequence Identity
GC Content (mean)
Genome Blast Coverage
Phylogenetic Signal
Intergenic Distance Evidence
Assembly Gaps
Synteny Proof (Interchromosomal)
Synteny Proof (Intrachromosomal)
5, 5, 5, 2
Set size
Evidence
Evidence Score
B
Max. Coverage (%)
Seq. Identity (%)
GC-content (%)
GC-Stretch

GC-content = 55.30 %
GC-content = 55.56 %
Human paralogue transcript ID (ranked by GC content)
Gene stable ID (ranked by GC content)
0
50
100
150
200
0
10
20
30
40
NOTCH2
KREMEN1
ADAP2
SLC9A5
MATK
MAN2B2
SSTR4
DNM3
STAP1
DNM3
HHLA2
SUV39H2
ADRA1B
GRK4
GPR78
HSD17B1
UNKL
SH2D2A
DIP2A
SIAH3
WNT2
KDM3A
RBBP7
HPGDS
IL13RA2
CAV3
SH2D1A
YBX3
IL5RA
MOB1A
SLC24A1
ELOVL3
FREM2
STOML3
LCP1
INTS6
ARL11
TBC1D14
GPR82
LRCH1
IL5RA
GPR82
Gene.name
ADAP2
ADRA1B
ARL11
CAV3
DIP2A
DNM3
ELOVL3
FREM2
GPR78
GPR82
GRK4
HHLA2
HPGDS
HSD17B1
IL13RA2
IL5RA
INTS6
KDM3A
KREMEN1
LCP1
LRCH1
MAN2B2
MATK
MOB1A
NOTCH2
RBBP7
SH2D1A
SH2D2A
SIAH3
SLC24A1
SLC9A5
SSTR4
STAP1
STOML3
SUV39H2
TBC1D14
UNKL
WNT2
YBX3
% Sequence identity (Human gene vs Paralog)
0–25%
25–50%
50–75%
75–100%

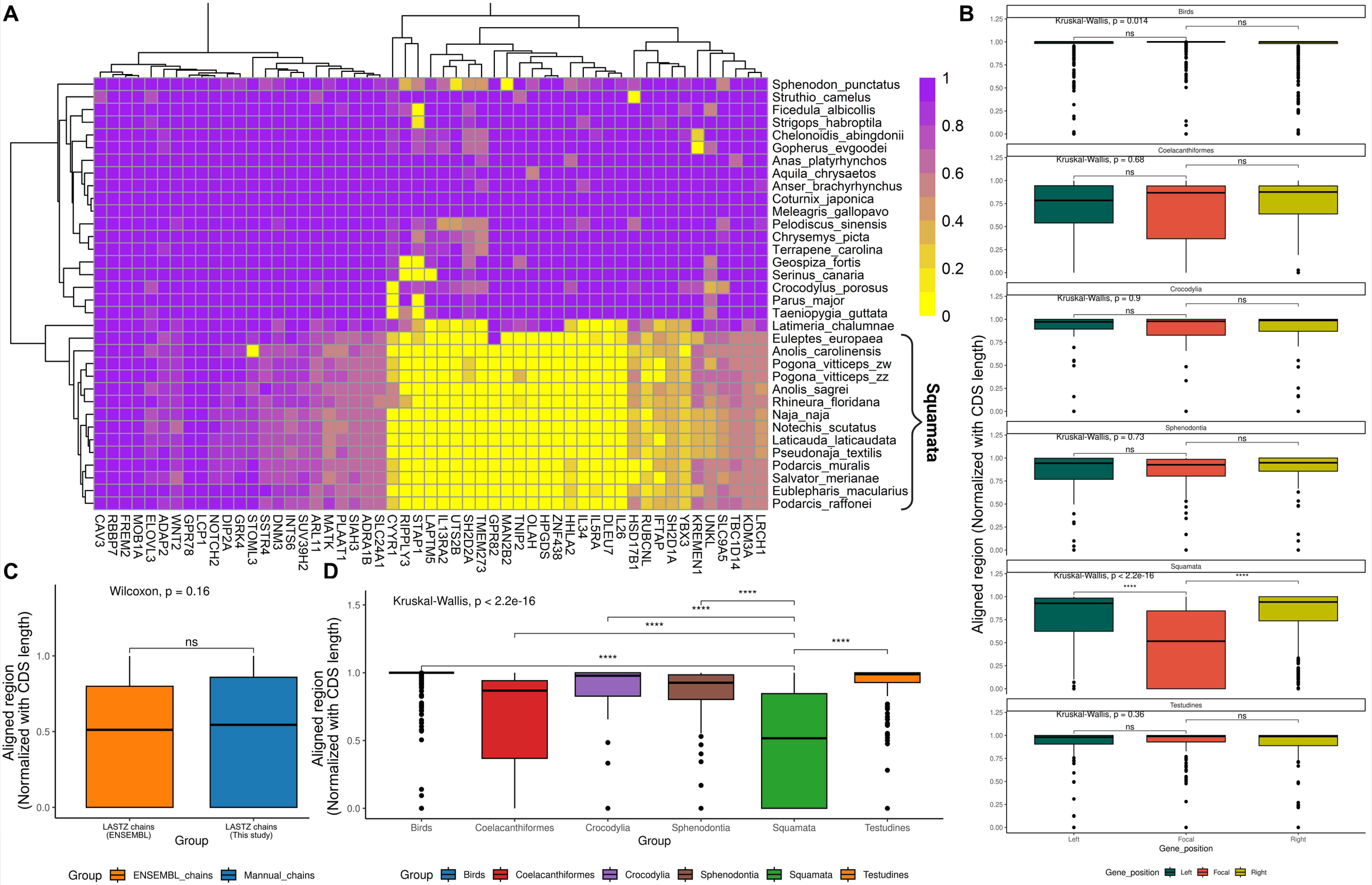
A
Sphenodon_punctatus
Struthio_camelus
Ficedula_albicollis
Strigops_habroptila
Chelonoidis_abingdonii
Gopherus_evgoodei
Anas_platyrhynchos
Aquila_chrysaetos
Anser_brachyrhynchus
Coturnix_japonica
Meleagris_gallopavo
Pelodiscus_sinensis
Chrysemys_picta
Terrapene_carolina
Geospiza_fortis
Serinus_canaria
Crocodylus_porosus
Parus_major
Taeniopygia_guttata
Latimeria_chalumnae
Euleptes_europaea
Anolis_carolinensis
Pogona_vitticeps_zw
Pogona_vitticeps_zz
Anolis_sagrei
Rhineura_floridana
Naja_naja
Notechis_scutatus
Laticauda_laticaudata
Pseudonaja_textilis
Podarcis_muralis
Salvator_merianae
Eublepharis_macularius
Podarcis_raffonei
Squamata
1
0.8
0.6
0.4
0.2
0
CAV3
RBBP7
FREM2
MOB1A
ELOVL3
ADAP2
WNT2
GPR78
LCP1
NOTCH2
DIP2A
GRK4
STOML3
SSTR4
DNM3
INTS6
SUV39H2
ARL11
MATK
PLAAT1
SIAH3
ADRA1B
SLC24A1
CYYR1
RIPPLY3
STAP1
LAPTM5
IL13RA2
UTS2B
SH2D2A
TMEM273
GPR82
MAN2B2
TNIP2
OLAH
HPGDS
ZNF438
HHLA2
IL34
IL5RA
DLEU7
IL26
HSD17B1
RUBCNL
IFTAP
SH2D1A
YBX3
KREMEN1
UNKL
SLC9A5
TBC1D14
KDM3A
LRCH1
B
Birds
Kruskal-Wallis, p = 0.014
Coelacanthiformes
Kruskal-Wallis, p = 0.68
Crocodylia
Kruskal-Wallis, p = 0.9
Sphenodontia
Kruskal-Wallis, p = 0.73
Squamata
Kruskal-Wallis, p < 2.2e-16
Testudines
Kruskal-Wallis, p = 0.36
ns
****
Aligned region (Normalized with CDS length)
Left
Focal
Right
Gene_position
C
Wilcoxon, p = 0.16
ns
Aligned region (Normalized with CDS length)
LASTZ chains (ENSEMBL)
LASTZ chains (This study)
Group
Group ENSEMBL_chains Mannual_chains
D
Kruskal-Wallis, p < 2.2e-16
****
Aligned region (Normalized with CDS length)
Birds
Coelacanthiformes
Crocodylia
Sphenodontia
Squamata
Testudines
Group
Group Birds Coelacanthiformes Crocodylia Sphenodontia Squamata Testudines

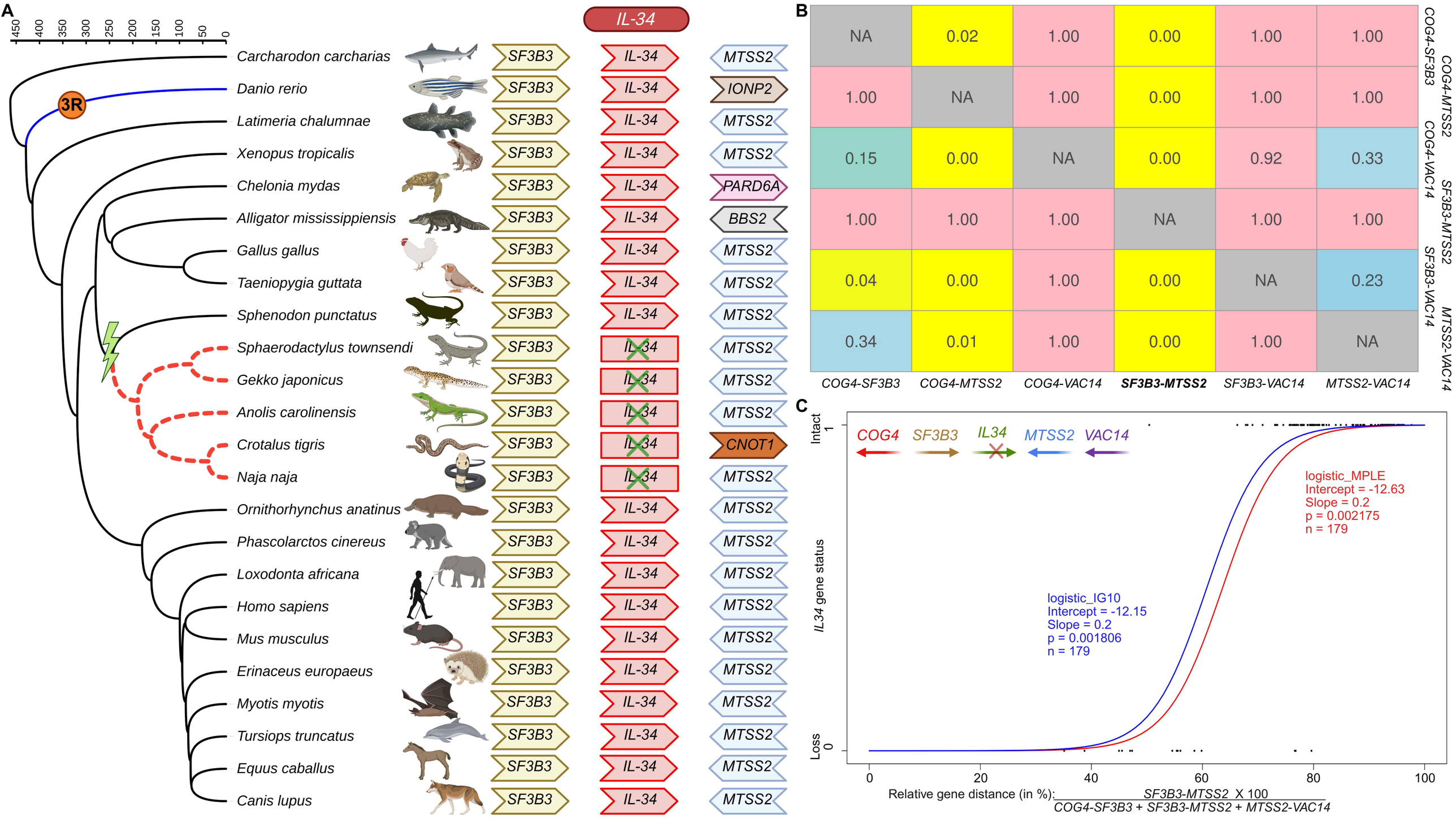
A
450
400
350
300
250
200
150
100
50
0
3R
IL-34
Carcharodon carcharias
Danio rerio
Latimeria chalumnae
Xenopus tropicalis
Chelonia mydas
Alligator mississippiensis
Gallus gallus
Taeniopygia guttata
Sphenodon punctatus
Sphaerodactylus townsendi
Gekko japonicus
Anolis carolinensis
Crotalus tigris
Naja naja
Ornithorhynchus anatinus
Phascolarctos cinereus
Loxodonta africana
Homo sapiens
Mus musculus
Erinaceus europaeus
Myotis myotis
Tursiops truncatus
Equus caballus
Canis lupus
SF3B3
IL-34
MTSS2
IONP2
PARD6A
BBS2
CNOT1
B
COG4-SF3B3
COG4-MTSS2
COG4-VAC14
SF3B3-MTSS2
SF3B3-VAC14
MTSS2-VAC14
NA 0.02 1.00 0.00 1.00 1.00
1.00 NA 1.00 0.00 1.00 1.00
0.15 0.00 NA 0.00 0.92 0.33
1.00 1.00 1.00 NA 1.00 1.00
0.04 0.00 1.00 0.00 NA 0.23
0.34 0.01 1.00 0.00 1.00 NA
C
Intact
Loss
IL34 gene status
COG4
SF3B3
IL34
MTSS2
VAC14
logistic_MPLE
Intercept = -12.63
Slope = 0.2
p = 0.002175
n = 179
logistic_IG10
Intercept = -12.15
Slope = 0.2
p = 0.001806
n = 179
0
20
40
60
80
100
Relative gene distance (in %): SF3B3-MTSS2 X 100 / COG4-SF3B3 + SF3B3-MTSS2 + MTSS2-VAC14

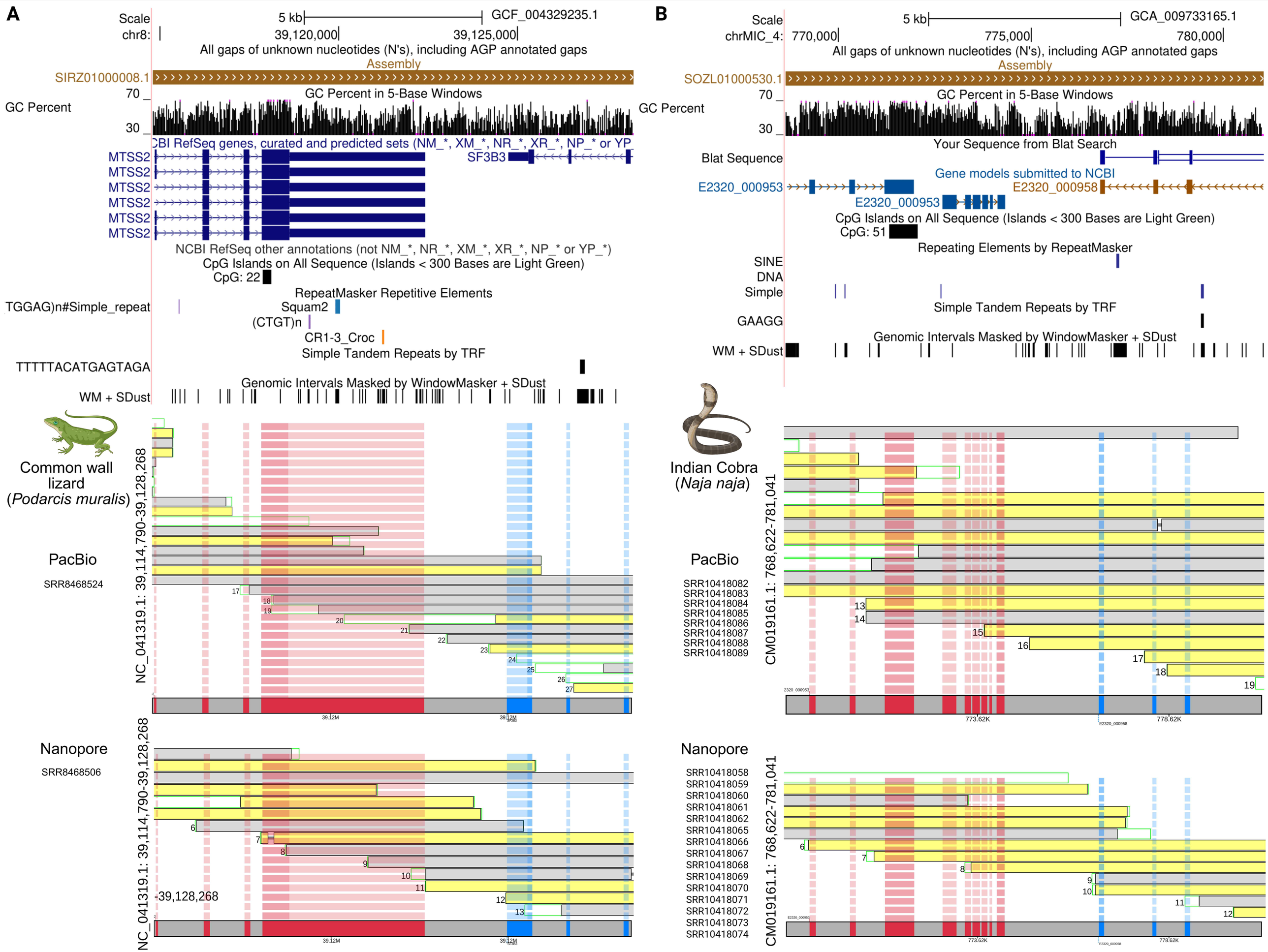
A
Scale
chr8:
5 kb
GCF_004329235.1
39,120,000
39,125,000
All gaps of unknown nucleotides (N's), including AGP annotated gaps
Assembly
SIRZ01000008.1
GC Percent in 5-Base Windows
GC Percent
70
30
CBI RefSeq genes, curated and predicted sets (NM_*, XM_*, NR_*, XR_*, NP_* or YP
MTSS2
SF3B3
NCBI RefSeq other annotations (not NM_*, NR_*, XM_*, XR_*, NP_* or YP_*)
CpG Islands on All Sequence (Islands < 300 Bases are Light Green)
CpG: 22
RepeatMasker Repetitive Elements
TGGAG)n#Simple_repeat
Squam2
(CTGT)n
CR1-3_Croc
Simple Tandem Repeats by TRF
TTTTTACATGAGTAGA
Genomic Intervals Masked by WindowMasker + SDust
WM + SDust
Common wall lizard (Podarcis muralis)
PacBio
SRR8468524
NC_041319.1: 39,114,790-39,128,268
Nanopore
SRR8468506
-39,128,268
39.12M
B
Scale
chrMIC_4:
5 kb
GCA_009733165.1
770,000
775,000
780,000
All gaps of unknown nucleotides (N's), including AGP annotated gaps
Assembly
SOZL01000530.1
GC Percent in 5-Base Windows
GC Percent
70
30
Your Sequence from Blat Search
Blat Sequence
Gene models submitted to NCBI
E2320_000953
E2320_000958
CpG Islands on All Sequence (Islands < 300 Bases are Light Green)
CpG: 51
Repeating Elements by RepeatMasker
SINE
DNA
Simple
Simple Tandem Repeats by TRF
GAAGG
Genomic Intervals Masked by WindowMasker + SDust
WM + SDust
Indian Cobra (Naja naja)
PacBio
SRR10418082
SRR10418083
SRR10418084
SRR10418085
SRR10418086
SRR10418087
SRR10418088
SRR10418089
CM019161.1: 768,622-781,041
773.62K
778.62K
Nanopore
SRR10418058
SRR10418059
SRR10418060
SRR10418061
SRR10418062
SRR10418065
SRR10418066
SRR10418067
SRR10418068
SRR10418069
SRR10418070
SRR10418071
SRR10418072
SRR10418073
SRR10418074

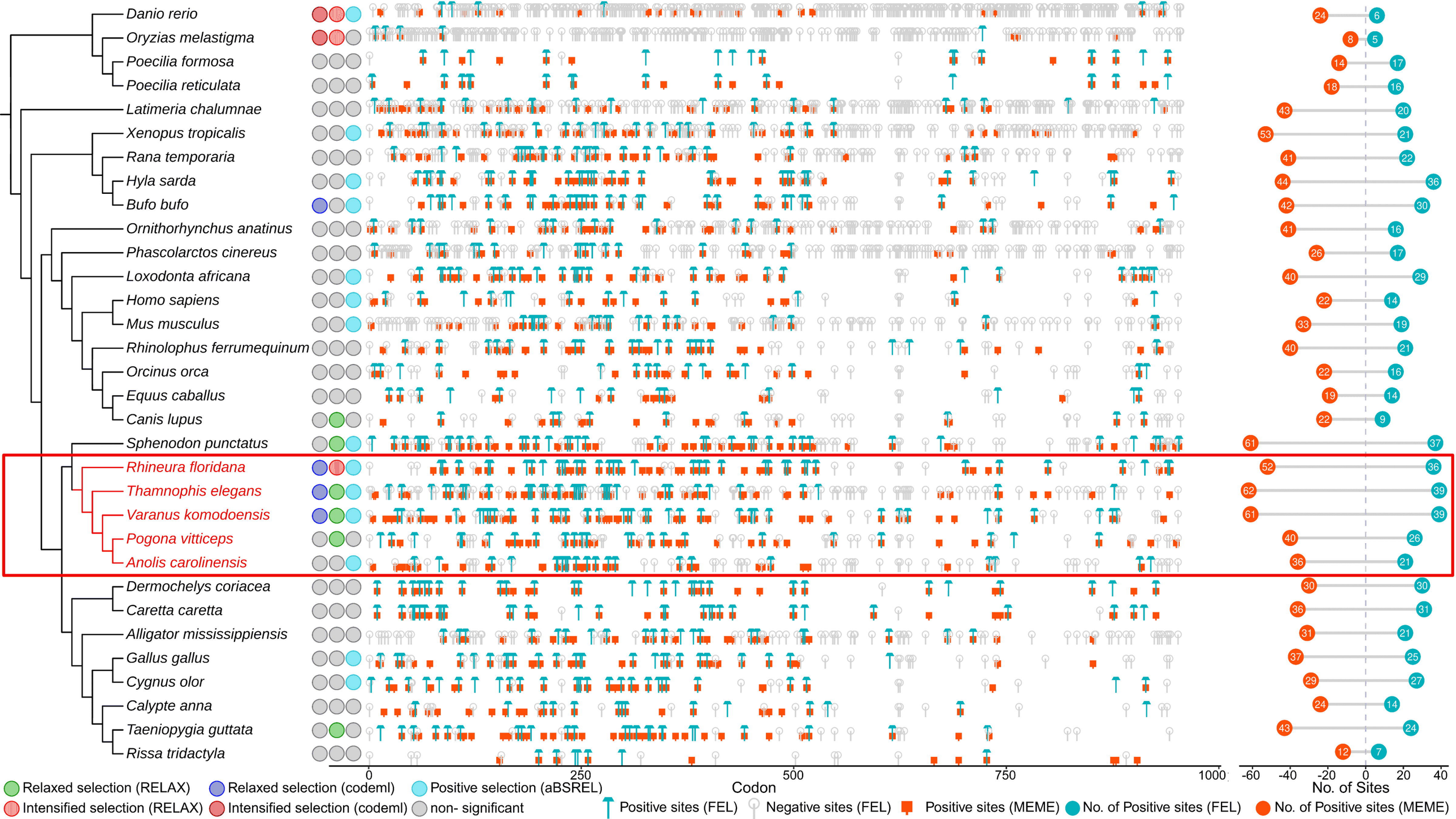
Danio rerio
Oryzias melastigma
Poecilia formosa
Poecilia reticulata
Latimeria chalumnae
Xenopus tropicalis
Rana temporaria
Hyla sarda
Bufo bufo
Ornithorhynchus anatinus
Phascolarctos cinereus
Loxodonta africana
Homo sapiens
Mus musculus
Rhinolophus ferrumequinum
Orcinus orca
Equus caballus
Canis lupus
Sphenodon punctatus
Rhineura floridana
Thamnophis elegans
Varanus komodoensis
Pogona vitticeps
Anolis carolinensis
Dermochelys coriacea
Caretta caretta
Alligator mississippiensis
Gallus gallus
Cygnus olor
Calypte anna
Taeniopygia guttata
Rissa tridactyla
0
250
500
750
1000
Codon
-60
-40
-20
0
20
40
No. of Sites
Relaxed selection (RELAX)
Relaxed selection (codeml)
Positive selection (aBSREL)
Intensified selection (RELAX)
Intensified selection (codeml)
non- significant
Positive sites (FEL)
Negative sites (FEL)
Positive sites (MEME)
No. of Positive sites (FEL)
No. of Positive sites (MEME)

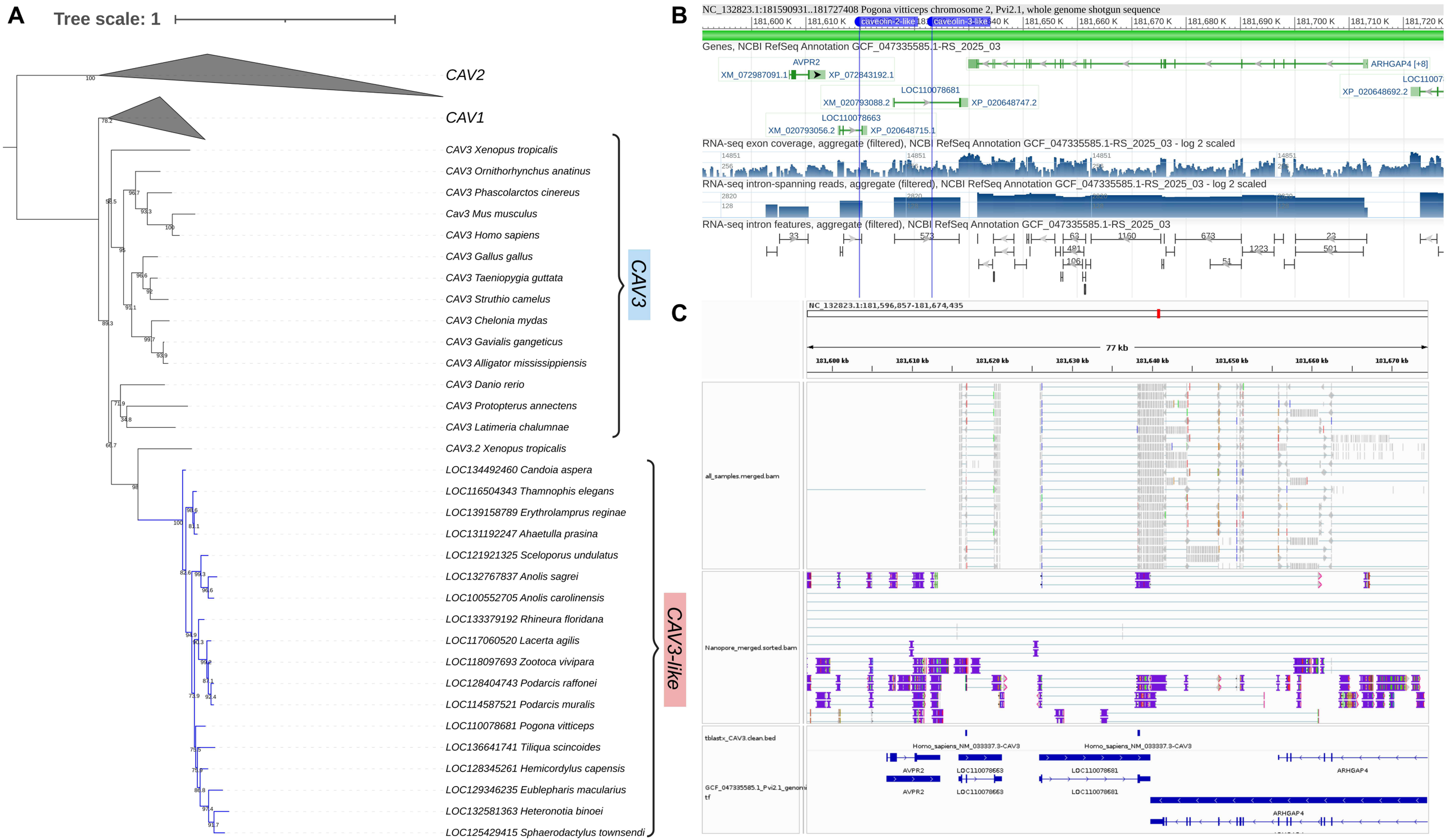
A
Tree scale: 1
CAV2
CAV1
CAV3 Xenopus tropicalis
CAV3 Ornithorhynchus anatinus
CAV3 Phascolarctos cinereus
Cav3 Mus musculus
CAV3 Homo sapiens
CAV3 Gallus gallus
CAV3 Taeniopygia guttata
CAV3 Struthio camelus
CAV3 Chelonia mydas
CAV3 Gavialis gangeticus
CAV3 Alligator mississippiensis
CAV3 Danio rerio
CAV3 Protopterus annectens
CAV3 Latimeria chalumnae
CAV3.2 Xenopus tropicalis
LOC134492460 Candoia aspera
LOC116504343 Thamnophis elegans
LOC139158789 Erythrolamprus reginae
LOC131192247 Ahaetulla prasina
LOC121921325 Sceloporus undulatus
LOC132767837 Anolis sagrei
LOC100552705 Anolis carolinensis
LOC133379192 Rhineura floridana
LOC117060520 Lacerta agilis
LOC118097693 Zootoca vivipara
LOC128404743 Podarcis raffonei
LOC114587521 Podarcis muralis
LOC110078681 Pogona vitticeps
LOC136641741 Tiliqua scincoides
LOC128345261 Hemicordylus capensis
LOC129346235 Eublepharis macularius
LOC132581363 Heteronotia binoei
LOC125429415 Sphaerodactylus townsendi
CAV3
CAV3-like
B
NC_132823.1:181590931..181727408 Pogona vitticeps chromosome 2, Pvi2.1, whole genome shotgun sequence
caveolin-2-like
caveolin-3-like
Genes, NCBI RefSeq Annotation GCF_047335585.1-RS_2025_03
AVPR2
XM_072987091.1
XP_072843192.1
ARHGAP4 [+8]
LOC110078681
XM_020793088.2
XP_020648747.2
XP_020648692.2
LOC110078663
XM_020793056.2
XP_020648715.1
RNA-seq exon coverage, aggregate (filtered), NCBI RefSeq Annotation GCF_047335585.1-RS_2025_03 - log 2 scaled
RNA-seq intron-spanning reads, aggregate (filtered), NCBI RefSeq Annotation GCF_047335585.1-RS_2025_03 - log 2 scaled
RNA-seq intron features, aggregate (filtered), NCBI RefSeq Annotation GCF_047335585.1-RS_2025_03
C
NC_132823.1:181,596,857-181,674,435
77 kb
all_samples.merged.bam
Nanopore_merged.sorted.bam
tblastx_CAV3.clean.bed
Homo_sapiens_NM_033337.3-CAV3
AVPR2
LOC110078663
LOC110078681
ARHGAP4
GCF_047335585.1_Pvi2.1_genomic.gff